Molecular Therapy
Original Article

Cholesterol-Lowering Gene Therapy Counteracts the Development of Non-ischemic Cardiomyopathy in Mice

Ilayaraja Muthuramu,[1] Ruhul Amin,[1] Andrey Postnov,[2] Mudit Mishra,[1] Joseph Pierre Aboumsallem,[1] Tom Dresselaers,[3,4] Uwe Himmelreich,[3] Paul P. Van Veldhoven,[5] Olivier Gheysens,[2] Frank Jacobs,[1] and Bart De Geest[1]

[1]Centre for Molecular and Vascular Biology, Department of Cardiovascular Sciences, Catholic University of Leuven, 3000 Leuven, Belgium; [2]Nuclear Medicine & Molecular Imaging, Department of Imaging & Pathology, Catholic University of Leuven, 3000 Leuven, Belgium; [3]Biomedical MRI, Department of Imaging & Pathology, Catholic University of Leuven, 3000 Leuven, Belgium; [4]Department of Radiology, University Hospitals Leuven, 3000 Leuven, Belgium; [5]Laboratory of Lipid Biochemistry and Protein Interactions, Department of Cellular and Molecular Medicine, Catholic University of Leuven, 3000 Leuven, Belgium

A causal role of hypercholesterolemia in non-ischemic heart failure has never been demonstrated. Adeno-associated viral serotype 8 (AAV8)-*low-density lipoprotein receptor* (AAV8-*LDLr*) gene transfer was performed in LDLr-deficient mice without and with pressure overload induced by transverse aortic constriction (TAC). AAV8-*LDLr* gene therapy resulted in an 82.8% ($p < 0.0001$) reduction of plasma cholesterol compared with controls. Mortality rate was lower ($p < 0.05$) in AAV8-LDLr TAC mice compared with control TAC mice (hazard ratio for mortality 0.457, 95% confidence interval [CI] 0.237–0.882) during 8 weeks of follow-up. AAV8-*LDLr* gene therapy attenuated cardiac hypertrophy, reduced interstitial and perivascular fibrosis, and decreased lung congestion in TAC mice. Cardiac function, quantified by invasive hemodynamic measurements and magnetic resonance imaging, was significantly improved 8 weeks after sham operation or after TAC in AAV8-LDLr mice compared with respective control groups. Myocardial protein levels of mammalian target of rapamycin and of acetyl-coenzyme A carboxylase were strikingly decreased following cholesterol lowering in mice without and with pressure overload. AAV8-LDLr therapy potently reduced cardiac glucose uptake and counteracted metabolic remodeling following pressure overload. Furthermore, oxidative stress and myocardial apoptosis were decreased following AAV8-LDLr therapy in mice with pressure overload. In conclusion, cholesterol-lowering gene therapy potently counteracts structural and metabolic remodeling, and enhances cardiac function.

INTRODUCTION

Epidemiological studies support a strong association between non-high-density lipoprotein (non-HDL) cholesterol levels and heart failure incidence. In Framingham Heart Study participants free of coronary heart disease at baseline, high non-HDL cholesterol levels were independently associated with heart failure incidence after adjustment for interim myocardial infarction and clinical covariates.[1] The results of the controlled rosuvastatin multinational study in heart failure (CORONA) randomized clinical trial[2] and the Gruppo Italiano per lo Studio della Sopravvivenza nella Insuffienza Cardiaca-heart failure (GISSI-HF) trial[3] evaluating the effect of 10 mg of rosuvastatin in patients with established chronic heart failure do not support a role for cholesterol-lowering therapies in the management of these patients. However, statins not only inhibit the synthesis of cholesterol, but also interfere with isoprenoid synthesis and the synthesis of isopentenyl pyrophosphate,[4,5] which may result in untoward myocardial effects unrelated to cholesterol lowering.

It has previously been demonstrated that a high-fat/high-cholesterol diet in pigs results in hyperactive mammalian target of rapamycin (mTOR) signaling in the heart,[6] which may have been directly related to hypercholesterolemia in these pigs. Because the mTOR complex 1 (mTORC1) promotes protein synthesis and cell growth, inhibits autophagy, and results in increased glucose oxidation and reduced fatty acid oxidation,[7,8] we hypothesized that cholesterol lowering per se may beneficially affect cardiac function via profound effects on myocardial metabolic remodeling. In addition, because oxidative stress may be critical for activation of apoptosis in the overloaded heart and cardiac cell death may contribute to deterioration of cardiac function,[9] reduction of oxidative stress following cholesterol lowering may counteract the progression of heart failure. To investigate the effect of cholesterol-lowering gene therapy, we performed adeno-associated viral serotype 8 (AAV8)-*low-density lipoprotein receptor (LDLr)* gene transfer in LDLr-deficient mice. The objective of the current study was to evaluate the effect of cholesterol-lowering gene therapy on structural and metabolic

Received 9 February 2017; accepted 27 July 2017;
http://dx.doi.org/10.1016/j.ymthe.2017.07.017.

Correspondence: Bart De Geest, MD, PhD, Centre for Molecular and Vascular Biology, Department of Cardiovascular Sciences, Catholic University of Leuven, Campus Gasthuisberg, Herestraat 49 bus 911, 3000 Leuven, Belgium.
E-mail: bart.degeest@kuleuven.be

remodeling and cardiac function in C57BL/6 LDLr$^{-/-}$ mice in the absence and presence of pressure overload induced by transverse aortic constriction (TAC).

RESULTS

AAV8-LDLr Gene Transfer Potently Lowers Lipoprotein Cholesterol Levels in C57BL/6 LDLr$^{-/-}$ Mice

All female C57BL/6 LDLr$^{-/-}$ mice in this study were fed standard chow supplemented with 0.2% cholesterol 10% coconut oil from the age of 12 weeks to induce hypercholesterolemia, and this diet was continued for the entire duration of the experiment. Total and non-HDL, very low-density lipoprotein (VLDL), intermediate-density lipoprotein (IDL), LDL, and HDL plasma cholesterol (mg/dL) at day 10 after saline injection or gene transfer are shown in Table S1. AAV8-*LDLr* gene transfer resulted in an 82.8% ($p < 0.0001$) reduction of plasma cholesterol levels compared with controls. Non-HDL, VLDL, IDL, and LDL cholesterol levels were 90.9% ($p < 0.0001$), 90.9% ($p < 0.0001$), 93.4% ($p < 0.0001$), and 87.6% ($p < 0.0001$) lower in AAV8-LDLr mice than in controls. HDL cholesterol levels were 35.8% ($p < 0.001$) decreased in AAV8-LDLr mice compared with controls. Cholesterol levels were stable for the entire duration of the experiment (data not shown). Plasma total cholesterol, non-HDL cholesterol, and HDL cholesterol values in AAV8-LDLr C57BL/6 LDLr$^{-/-}$ mice (Table S1) were very similar compared with reference C57BL/6 mice ($n = 10$) (total cholesterol 66.5 ± 3.3 mg/dL; non-HDL cholesterol 23.7 ± 2.6 mg/dL; HDL cholesterol 42.8 ± 3.5 mg/dL).

Murine LDLr expression in the liver of C57BL/6 mice, C57BL/6 LDLr$^{-/-}$ mice, and C57BL/6 LDLr$^{-/-}$ mice treated with 2×10^{12} genome copies/kg AAV8-LDLr is illustrated in Figure S1. Murine LDLr was undetectable in C57BL/6 LDLr$^{-/-}$ mice. Murine LDLr expression 10 weeks after gene transfer with AAV8-LDLr in C57BL/6 LDLr$^{-/-}$ mice was 1.56-fold ($p < 0.01$) higher compared with wild-type C57BL/6 mice.

Myocardial lipid levels 8 weeks after sham operation or after TAC in C57BL/6 LDLr$^{-/-}$ mice are shown in Table S2. No significant differences in total myocardial cholesterol levels were observed. Myocardial cholesteryl esters were reduced by 46.0% ($p < 0.05$) in AAV8-LDLr sham mice and by 76.4% ($p < 0.05$) in AAV8-LDLr TAC mice compared with respective control groups. Myocardial sphingomyelin was increased by 37.8% ($p < 0.05$) in control TAC mice compared with control sham mice (Table S2).

Cholesterol-Lowering Gene Transfer Reduces Mortality after TAC

TAC was performed at the age of 17 weeks to induce pressure overload. Comparison of Kaplan-Meier survival curves showed a significantly ($p < 0.05$) decreased mortality rate in AAV8-LDLr TAC mice compared with control TAC mice (hazard ratio for mortality 0.457, 95% confidence interval [CI] 0.237–0.882) during a follow-up period of 8 weeks (Figure S2). Sham operation did not result in any mortality (data not shown).

Cholesterol-Lowering Gene Transfer Attenuates Cardiac Hypertrophy and Decreases Lung Congestion after TAC

No significant differences in body weight (Figure 1A) and tibia length (Figure 1B) were observed between different groups. The heart weight was 2.21-fold ($p < 0.001$) higher in control TAC mice and 1.79-fold ($p < 0.001$) higher in AAV8-LDLr TAC mice compared with respective sham groups (Figure 1C). Cholesterol lowering attenuated cardiac hypertrophy as evidenced by a 20.0% ($p < 0.01$) lower heart weight in AAV8-LDLr TAC than in control TAC mice. Left ventricular weight at sacrifice (Figure 1D) and quantified by magnetic resonance imaging (Figure 1E) was significantly lower in AAV8-LDLr TAC mice than in control TAC mice. Histological analysis demonstrated a 14.5% ($p < 0.001$) smaller left ventricular wall area (Figure 1F) and a 15.5% ($p < 0.05$) reduction of cardiomyocyte cross-sectional area in AAV8-LDLr TAC mice than in control TAC mice (Figure 1G). Cholesterol-lowering gene therapy also significantly ($p < 0.05$) reduced cardiomyocyte cross-sectional area in sham mice (Figure 1G). Furthermore, right ventricular hypertrophy was observed in control TAC mice as evidenced by a 1.77-fold ($p < 0.01$) increase of right ventricular weight compared with the control sham group (Figure 1H). In contrast, no significant hypertrophy of the right ventricle was observed in AAV8-LDLr TAC mice (Figure 1H). Lung weight was 2.00-fold ($p < 0.01$) higher in the control TAC group compared with the control sham group (Figure 1I). Cholesterol-lowering gene transfer decreased lung congestion after TAC as evidenced by a 38.6% ($p < 0.05$) lower lung weight in AAV8-LDLr TAC mice than in control TAC mice (Figure 1I).

Representative Sirius-red-stained cross sections of sham hearts and TAC hearts are illustrated in Figure S3. An overview of morphometric and histological parameters is shown in Table S3. Representative photomicrographs of immunohistochemical analyses are illustrated in Figure S4.

Sustained Akt activation induces cardiac hypertrophy, which may lead to heart failure. Myocardial Akt (Figure 2A) and p-Akt (Figure 2B) levels were reduced by 30.0% ($p < 0.01$) and 31.5% ($p < 0.01$) in AAV8-LDLr TAC mice compared with control TAC mice. Mammalian or mechanistic target of rapamycin (mTOR), involved in cell growth, autophagy, and metabolism, was reduced by 45.7% ($p < 0.05$) in AAV8-LDLr sham mice and by 32.5% ($p < 0.05$) in AAV8-LDLr TAC mice compared with respective control groups (Figure 2C). Myocardial levels of p-mTOR were 54.3% ($p < 0.05$) lower in AAV8-LDLr sham mice and 40.1% ($p < 0.05$) in AAV8-LDLr TAC mice than in respective control groups (Figure 2D). Mitogen-activated protein kinase (MAPK) kinase (MEK) protein levels (Figure 2E) and p-MEK levels (Figure 2F) were 36.6% ($p < 0.001$) and 30.2% ($p < 0.05$) lower in AAV8-LDLr TAC mice than in control TAC mice. Furthermore, cholesterol-lowering gene therapy decreased cardiac extracellular signal-regulated kinase (ERK) (Figure 2G), p-ERK (Figure 2H), c-Jun N-terminal kinase (JNK) (Figure 2I), and p-JNK (Figure 2J) levels after TAC compared with control TAC mice. In contrast, p38 MAPK (p38) (Figure 2K)

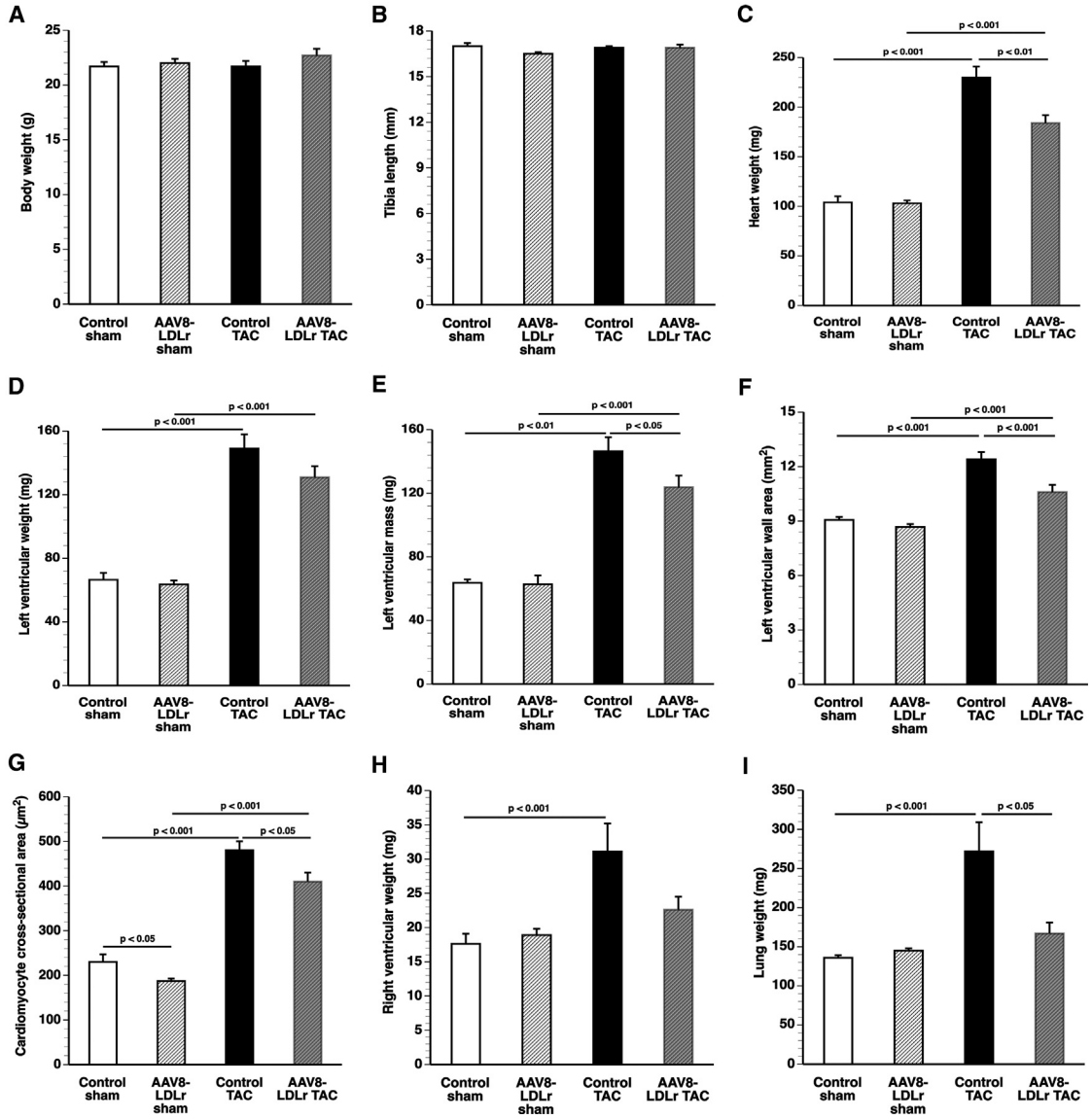

Figure 1. Cholesterol-Lowering Gene Therapy Attenuates Cardiac Hypertrophy and Lung Congestion after TAC

(A–D) Bar graphs illustrating body weight (A), tibia length (B), heart weight (C), and left ventricular weight (D) in control sham (n = 10), AAV8-LDLr sham (n = 10), control TAC (n = 11), and AAV8-LDLr TAC (n = 11) mice 8 weeks after operation. (E) Left ventricular mass quantified by micro-MRI (n = 6 in each group). (F and G) Left ventricular wall area (F) and cardiomyocyte cross-sectional area (G) quantified by morphometric and histological analysis in control sham (n = 15), AAV8-LDLr sham (n = 22), control TAC (n = 23), and AAV8-LDLr TAC (n = 23) mice 8 weeks after operation. (H and I) Bar graphs showing right ventricular weight (H) and wet lung weight (I) in control sham (n = 10), AAV8-LDLr sham (n = 10), control TAC (n = 11), and AAV8-LDLr TAC (n = 11) mice 8 weeks after operation. Error bars represent SEM.

and p-p38 MAPK levels (Figure 2L) were not significantly different between control TAC mice and AAV8-LDLr TAC mice. Representative images of western blots are shown in Figure 2M.

To confirm that the housekeeping protein glyceraldehyde 3-phosphate dehydrogenase (GAPDH) is an adequate reference for normalizing protein expression levels, we compared GAPDH and β-tubulin expression levels (Figure S5). GAPDH/β-tubulin ratios were highly similar between the four different groups, confirming that GAPDH is an adequate reference for normalizing protein expression levels (Figure S5).

Cholesterol-Lowering Gene Therapy Significantly Reduces Interstitial Fibrosis and Perivascular Fibrosis after TAC

The degree of interstitial fibrosis (Figure 3A) and perivascular fibrosis (Figure 3B) was reduced by 21.8% ($p < 0.05$) and 38.3% ($p < 0.01$) in AAV8-LDLr TAC mice compared with control TAC mice. Representative photomicrographs of Sirius-red-stained interstitial collagen

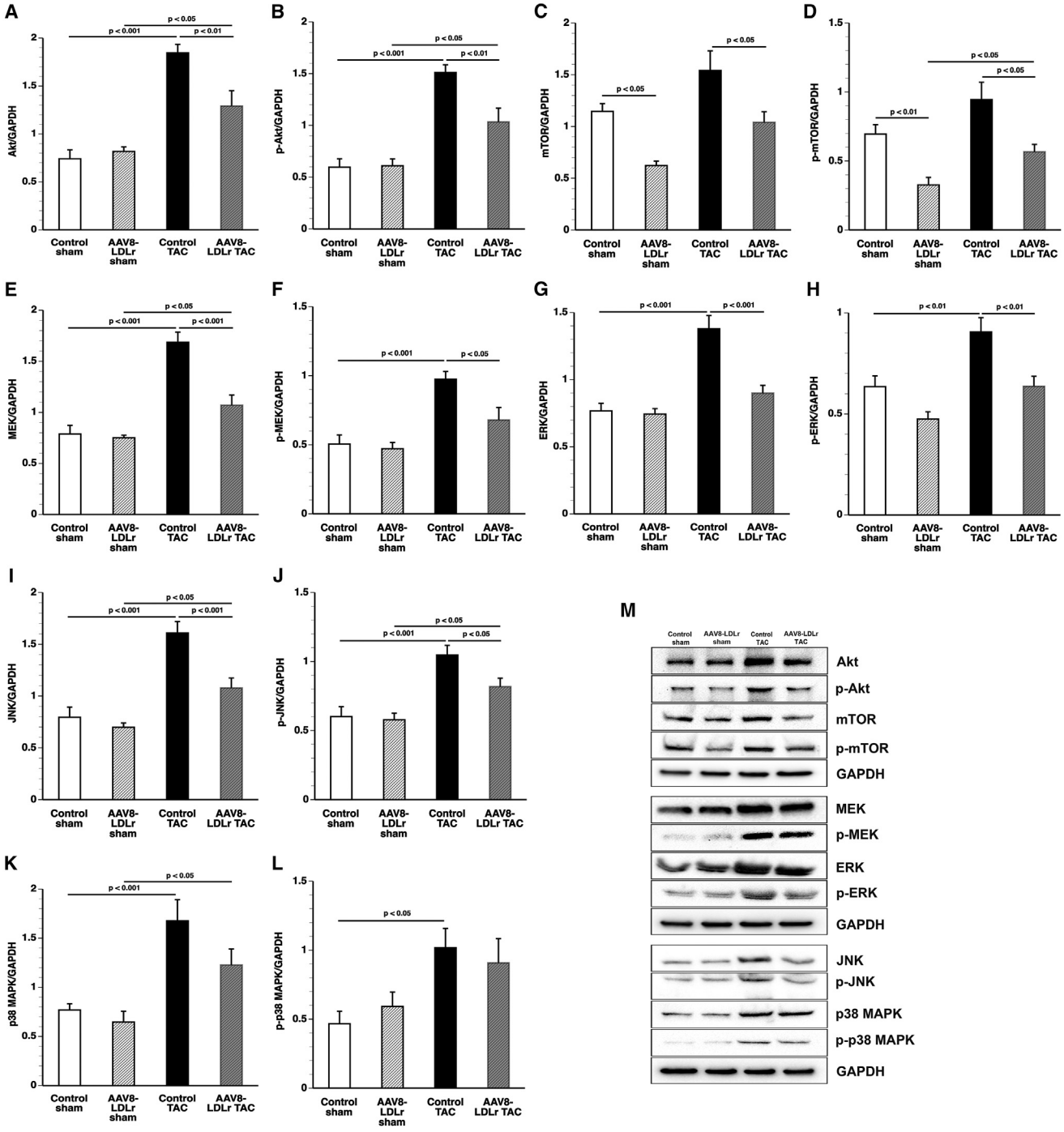

Figure 2. Quantification of Pro-hypertrophic Myocardial Proteins by Western Blot

(A–L) Bar graphs illustrating Akt (A), p-Akt (B), mTOR (C), p-mTOR (D), MEK (E), p-MEK (F), ERK (G), p-ERK (H), JNK (I), p-JNK (J), p38 (K), and p-p38 (L) protein levels quantified by western blot in the myocardium of control sham (n = 10), AAV8-LDLr sham (n = 10), control TAC (n = 9), and AAV8-LDLr TAC (n = 10) mice 8 weeks after operation. All protein levels were normalized to the glyceraldehyde-3-phosphate dehydrogenase (GAPDH) protein level. (M) Representative images of western blots are shown. Error bars represent SEM.

viewed under polarized light are shown in Figure 3C. The 12.5-kDa isoform of transforming growth factor β1 (TGF-β1) was reduced by 27.3% ($p < 0.001$) in AAV8-LDLr TAC mice compared with control TAC mice (Figure 3D). Cholesterol-lowering gene therapy reduced Smad1 (Figure 3E), p-Smad1/5 (Figure 3F), and Smad4 (Figure 3G) after TAC by 46.9% ($p < 0.01$), 49.7% ($p < 0.001$), and 48.7% ($p < 0.001$), respectively, compared with control TAC mice. Representative images of western blots are shown in Figure 3H.

Lowering of Cholesterol Improves Cardiac Function in the Absence and Presence of Pressure Overload

Systolic function and diastolic function 8 weeks after sham operation were significantly improved in AAV8-LDLr sham mice compared with control sham mice as evidenced by the increased peak rate of isovolumetric contraction (dP/dt_{max}), a more negative peak rate of isovolumetric relaxation (dP/dt_{min}), and a smaller time constant of left ventricular isovolumetric relaxation (τ [tau]) (Table 1). The peak rate of isovolumetric contraction (dP/dt_{max}) was increased by 20.0% ($p < 0.05$) in AAV8-LDLr TAC mice compared with control TAC mice. The time constant of left ventricular relaxation (τ) was 13.2% ($p < 0.05$) lower in AAV8-LDLr TAC mice than in control TAC mice. The pressure gradient over TAC was quantified by measuring the difference of the systolic pressure in the right carotid artery and the left carotid artery. This gradient was similar in control TAC mice (88.6 ± 9.7 mm Hg; $n = 6$) compared with AAV8-LDLr mice (91.2 ± 9.4 mm Hg; $n = 6$). Taken together, AAV8-LDLr gene transfer results in improved systolic and diastolic function in both in sham mice and TAC mice.

The quantification of end-diastolic volume (EDV), end-systolic volume (ESV), stroke volume, and ejection fraction by micro-MRI is shown in Figure 4. The stroke volume was increased by 26.5% ($p < 0.05$) in AAV8-LDLr TAC mice compared with control TAC mice (Figure 4C). The ejection fraction was 1.54-fold ($p < 0.01$) lower in control TAC mice and 1.17-fold ($p < 0.05$) lower in AAV8-LDLr TAC mice compared with respective sham groups (Figure 4D).

Reduction of Cholesterol Counteracts Metabolic Remodeling Induced by Pressure Overload

Capillary glucose levels did not differ between the different experimental groups (Figure 5A). Plasma insulin was 1.90-fold ($p < 0.05$) higher in control TAC mice than in control sham mice (Figure 5B). Parameters of glucose uptake in the myocardium and the left quadriceps quantified by micro-positron emission tomography (micro-PET) imaging using [^{18}F]-fluorodeoxyglucose (FDG) as a tracer are shown in Figures 5C and 5D and in Table S4. TAC was associated with a significantly increased glucose uptake in the myocardium. The maximal standardized uptake value (SUV) was 2.12-fold ($p < 0.001$) higher in control TAC mice and 1.51-fold ($p < 0.05$) higher in AAV8-LDLr TAC mice than in respective sham groups. Maximal SUV was reduced by 29.5% ($p < 0.05$) in AAV8-LDLr TAC mice compared with control TAC mice. The total accumulation of glucose in the myocardium was 56.3% ($p < 0.05$) lower in AAV8-LDLr TAC mice than in control TAC mice. Taken together, increased glucose uptake in the myocardium after TAC is significantly attenuated following cholesterol-lowering gene therapy. Representative micro-PET images illustrating the myocardial uptake of [^{18}F]-FDG are shown in Figure 5E.

Pressure overload significantly increased myocardial GLUT4 protein levels (Figure 6A) and pyruvate dehydrogenase (PDH) levels (Figure 6B). Cholesterol-lowering gene transfer reduced GLUT4 protein levels by 18.0% ($p < 0.05$) and PDH levels by 33.3% ($p < 0.001$) compared with control TAC mice. Myocardial protein levels of PDH kinase (PDHK), which inactivates PDH, were reduced by 56.5% ($p < 0.001$) in control TAC mice compared with control sham mice and were 2.24-fold ($p < 0.001$) higher in AAV8-LDLr TAC mice than in control TAC mice (Figure 6C). Taken together, these data suggest that increased glucose uptake is accompanied by increased glucose oxidation in control TAC mice.

Myocardial AMP-activated protein kinase (AMPK) (Figure 6D) and p-AMPK (Figure 6E) protein levels were significantly lower in control TAC mice compared with control sham mice and AAV8-LDLr TAC mice. Levels of acetyl-coenzyme A (acetyl-CoA) carboxylase (ACC) (Figure 6F) were 34.4% lower in AAV8-LDLr TAC mice compared with control TAC mice. Levels of p-ACC (Figure 6G), which constitutes the inactive form of the enzyme, were significantly higher in AAV8-LDLr sham mice ($p < 0.001$) and AAV8-LDLr TAC mice ($p < 0.01$) compared with respective control groups. Myocardial protein levels of peroxisome proliferator-activated receptor (PPAR)-α, a key transcriptional factor regulating fatty acid oxidation, were 1.52-fold ($p < 0.01$) higher in AAV8-LDLr sham mice and 2.01-fold ($p < 0.001$) higher in AAV8-LDLr TAC mice compared with respective control groups (Figure 6H). PPAR-α levels were 32.3% ($p < 0.05$) lower in control TAC mice compared with control sham mice. Similar profound differences of expression levels were also observed for retinoid X receptor (RXR)-α, the heterodimerization partner of PPAR-α and of liver X receptor (LXR)-α and LXR-β (Figure S6A). Myocardial protein levels of carnitine palmitoyltransferase IB (CPT1B) were 1.97-fold ($p < 0.001$) higher in AAV8-LDLr TAC mice than in control TAC mice (Figure 6I). Similarly, protein levels of long-chain acyl-CoA synthetase, member 1 (ACSL1), and of long-chain acyl-CoA dehydrogenase (ACADL) were significantly ($p < 0.05$) higher in AAV8-LDLr TAC mice than in control TAC mice (Figures S6B and S6C). Moreover, ACADL levels were 1.61-fold ($p < 0.001$) higher in AAV8-LDLr sham mice than in control sham mice. Expression of CD36 or fatty acid translocase (FAT) was similar between different groups (Figure S6D). Myocardial protein levels of LXR-α and of LXR-β were significantly higher in AAV8-LDLr sham mice and in AAV8-LDLr TAC mice compared with respective control groups and were significantly lower in control TAC mice compared with control sham mice (Figures 6J and 6K). Levels of fatty acid synthase (FAS), an LXR target, were 2.59-fold ($p < 0.001$) higher in AAV8-LDLr TAC mice than in control TAC mice (Figure 6L). Representative images of western blots are shown in Figure 6M.

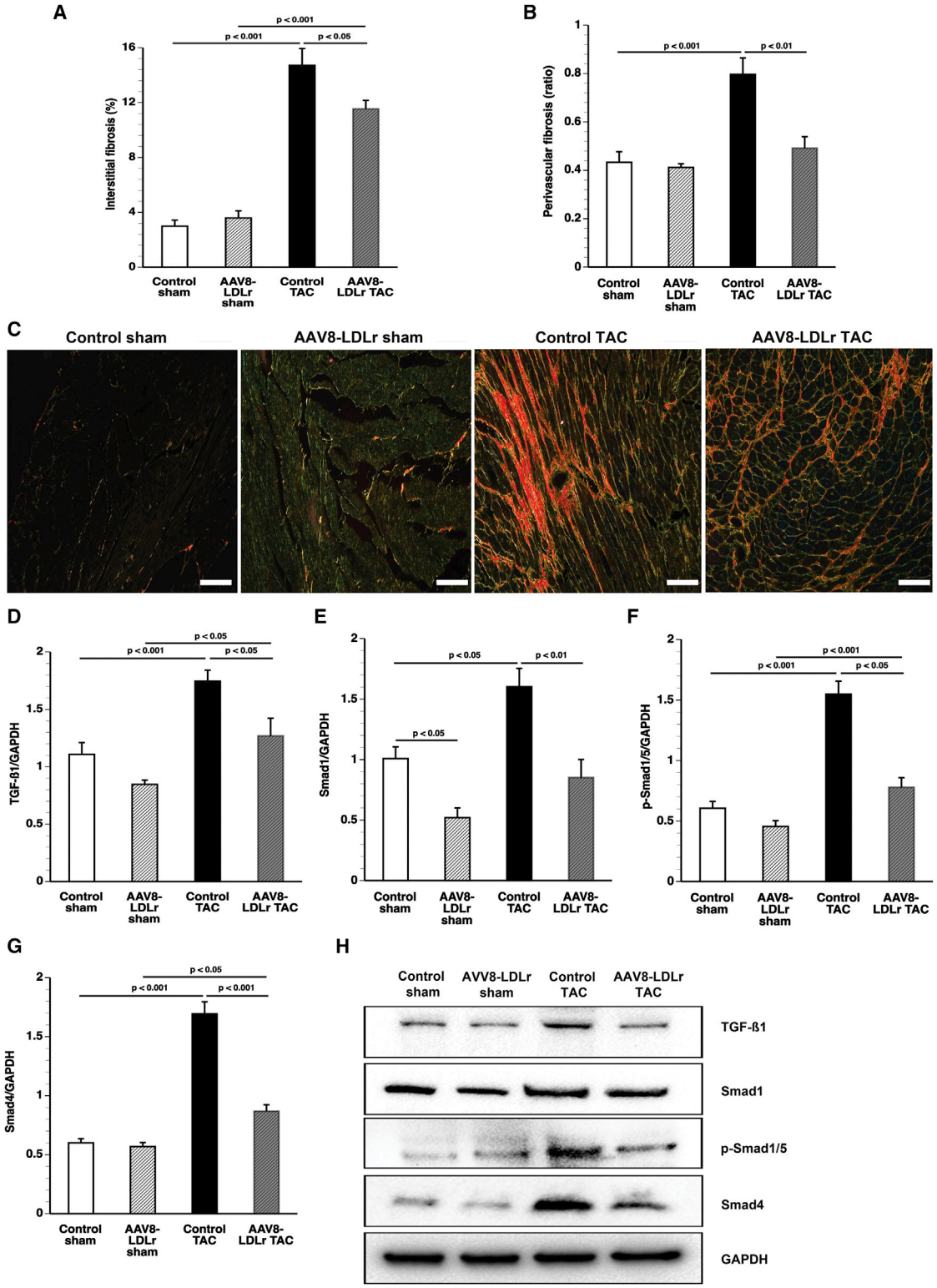

Figure 3. Cholesterol-Lowering Gene Transfer Significantly Reduces Interstitial Fibrosis and Perivascular Fibrosis after TAC

(A and B) Bar graphs illustrating the degree of interstitial fibrosis (A) and the degree of perivascular fibrosis (B) in control sham (n = 15), AAV8-LDLr sham (n = 22), control TAC (n = 23), and AAV8-LDLr TAC (n = 23) mice 8 weeks after operation. (C) Representative photomicrographs showing Sirius-red-stained interstitial collagen viewed under

(legend continued on next page)

Table 1. Hemodynamic Parameters in the Left Ventricle and in the Aorta 8 Weeks after Sham Operation and after TAC in C57BL/6 LDLr$^{-/-}$ Mice

	Control Sham	AAV8-LDLr Sham	Control TAC	AAV8-LDLr TAC
Number of mice	19	13	19	16
Left Ventricle				
Peak systolic pressure (mm Hg)	100 ± 1	103 ± 2	150 ± 8§§§	160 ± 9§§§
End-diastolic pressure (mm Hg)	2.15 ± 0.58	2.38 ± 0.35	3.64 ± 0.50	2.59 ± 0.84
dP/dt_{max} (mm Hg/ms)	9.76 ± 0.43	11.4 ± 0.3$^{°°}$	9.25 ± 0.47	11.1 ± 0.9*
dP/dt_{min} (mm Hg/ms)	−8.14 ± 0.31	−10.2 ± 0.2$^{°°°}$	−9.19 ± 0.55	−10.5 ± 0.8
τ (ms)	5.32 ± 0.20	4.65 ± 0.13°	5.70 ± 0.21	4.95 ± 0.21*
Heart rate (bpm)	599 ± 11	610 ± 10	580 ± 20	622 ± 10
Aorta				
Mean pressure (mm Hg)	80.8 ± 1.5	82.1 ± 2.1	87.7 ± 3.8	97.9 ± 5.5§
Systolic pressure (mm Hg)	99.2 ± 1.6	101 ± 2	147 ± 8§§§	155 ± 11§§§
Diastolic pressure (mm Hg)	64.7 ± 2.0	64.0 ± 3.5	50.6 ± 4.4§	60.5 ± 7.0

Data are expressed as means ± SEM. °$p < 0.05$, °°$p < 0.01$, °°°$p < 0.001$ versus control sham; $^{§}p < 0.05$, $^{§§§}p < 0.001$ versus respective sham groups; *$p < 0.05$ versus control TAC.

Oxidative Stress and Myocardial Apoptosis Are Reduced by Cholesterol-Lowering Gene Therapy in Mice with Chronic Pressure Overload

Plasma thiobarbituric acid reactive substances (TBARSs) and the 3-nitrotyrosine-positive area (%) in the myocardium are shown in Figures 7A and 7B, respectively. Plasma TBARSs were 74.7% ($p < 0.05$) higher in control TAC mice compared with control sham mice. A 39.6% ($p < 0.01$) reduction of plasma TBARSs was observed in AAV8-LDLr TAC mice compared with control TAC mice. Compared with respective sham groups, 3-nitrotyrosine-positive area (%) in the myocardium quantified by immunohistochemistry was increased 4.89-fold ($p < 0.001$) and 2.40-fold ($p < 0.001$) in control TAC mice and in AAV8-LDLr TAC mice, respectively. The 3-nitrotyrosine-positive area was 49.7% ($p < 0.001$) lower in AAV8-LDLr TAC mice than in control TAC mice, indicating decreased nitro-oxidative stress. Apoptosis in the myocardium was evaluated using immunohistochemical quantification of cleaved caspase-3. Cleaved caspase-3-positive cells were undetectable in the myocardium of sham mice (Figure 7C). Compared with control TAC mice, the number of cleaved caspase-3 positive cells was reduced by 43.0% ($p < 0.01$) in AAV8-LDLr TAC mice (Figure 7C). Representative myocardial sections immunostained for 3-nitrotyrosine are shown in Figure 7D.

DISCUSSION

The main findings of the current study are that cholesterol-lowering gene therapy attenuated cardiac hypertrophy, decreased interstitial fibrosis, counteracted metabolic remodeling, and lowered oxidative stress in mice with pressure overload. Systolic and diastolic cardiac functions were improved following AAV8-mediated *LDLr* gene transfer both in the absence and presence of pressure overload.

The impact of plasma cholesterol on cardiac function in the absence of coronary heart disease is not well established, and the effect of statins in the setting of heart failure is controversial. AAV8-*LDLr* gene transfer resulted in a very profound reduction of plasma cholesterol levels. Because cholesterol reduction in this study was achieved via AAV8-mediated *LDLr* gene transfer (and not, e.g., as a result of dietary manipulations that may result in non-selective effects), this strategy is appropriate to study the effect of cholesterol levels per se. In contrast, statins do not specifically lower plasma cholesterol, and pleiotropic effects of statins might be detrimental in the setting of heart failure. Endogenous coenzyme Q10 synthesis is blocked by 3-hydroxy-3-methylglutaryl-CoA reductase inhibitors (statins).[4] Coenzyme Q10 is a component of the electron transport chain and participates in aerobic cellular respiration. Low plasma coenzyme Q10 levels are a risk factor for worsened outcomes in heart failure.[10] In addition, blocking the mevalonate pathway by statins also inhibits the synthesis of isopentenyl pyrophosphate. This molecule is not only a building block for cholesterol, but is also required for the post-transcriptional enzymatic isopentenylation of selenocysteine tRNA and its maturation to a functional tRNA molecule. Inhibition of isopentenyl pyrophosphate synthesis by statins results in a decrease in available selenoproteins,[5] including glutathione peroxidases. A reduction of myocardial glutathione peroxidases may impair cardiac function via increased oxidative stress.[11]

The attenuation of cardiac hypertrophy induced by pressure overload in mice treated with AAV8-*LDLr* gene transfer is a striking observation in the current study. The mTOR pathway plays a key role in sensing and integrating multiple environmental signals.[12] The mTORC1 promotes protein synthesis and cell growth, inhibits

polarized light. Scale bars, 50 μm. (D–G) Bar graphs illustrating the 12.5-kDa isoform of TGF-β1 (D), Smad1 (E), p-Smad1/5 (F), and Smad4 (G) myocardial protein levels quantified by western blot in the myocardium of control sham (n = 10), AAV8-LDLr sham (n = 10), control TAC (n = 9), and AAV8-LDLr TAC (n = 10) mice 8 weeks after operation. All protein levels were normalized to the glyceraldehyde-3-phosphate dehydrogenase (GAPDH) protein level. (H) Representative images of western blots are shown. Error bars represent SEM.

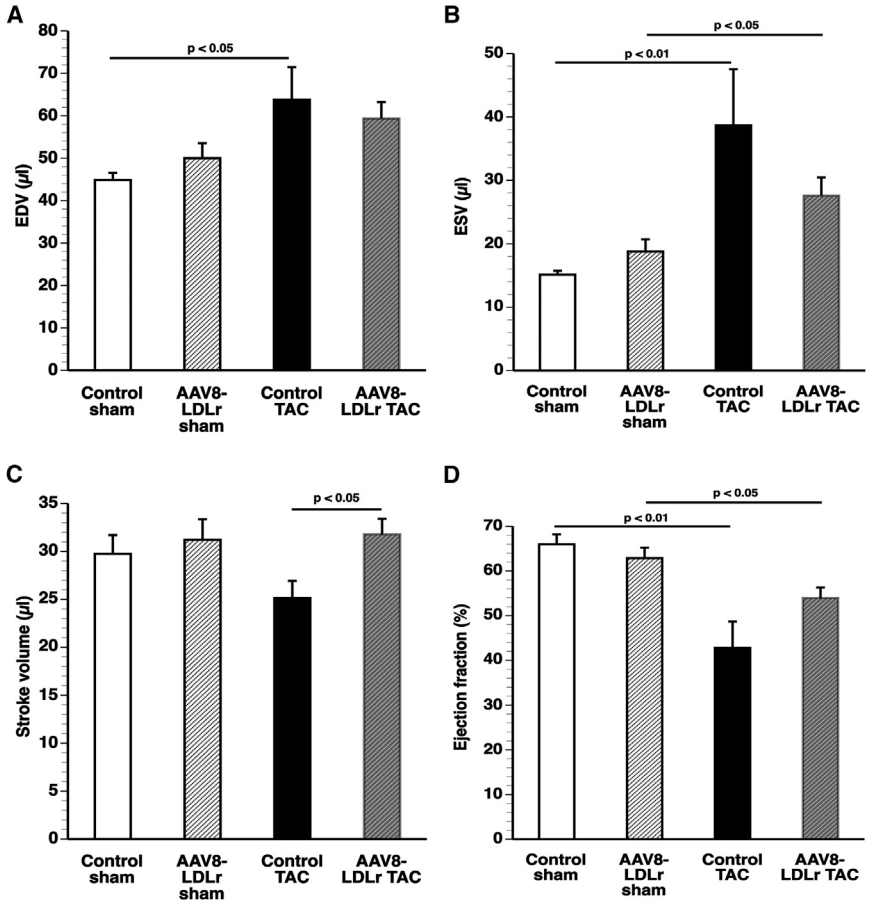

Figure 4. Cholesterol Lowering Increases Stroke Volume after TAC

(A–D) End-diastolic volume (EDV) (A), end-systolic volume (ESV) (B), stroke volume (C), and ejection fraction (D) in sham mice and in TAC mice (n = 6 for each group). Sham operation or TAC was performed at the age of 17 weeks. Micro-magnetic resonance imaging was performed 8 weeks later. Error bars represent SEM.

autophagy, and results in increased glucose oxidation and reduced fatty acid oxidation.[7,8] Whereas complete genetic disruption of mTORC1 impairs the capacity of the heart to respond to pressure overload and potentiates the development of dilated cardiomyopathy, partial inhibition of mTORC1 decreases cardiac hypertrophy and improves cardiac function in the presence of pressure overload.[13–15] Cholesterol trafficking has been shown to be required for mTOR activation.[12] An obvious upregulation of mTOR and p-mTOR protein in macrophage-derived foam cells generated using Cu^{2+}-oxidized LDL was observed by Wang et al.[16] and suggests a link between cholesteryl ester accumulation and mTOR expression. The decrease of myocardial cholesteryl ester levels following cholesterol-lowering gene transfer is consistent with altered intracellular cholesterol dynamics. This may directly underlie the fact that protein levels of mTOR and p-mTOR were strikingly decreased following cholesterol-lowering gene transfer both in the absence and presence of pressure overload. In mice with pressure overload, differential Akt and AMPK activity may also have contributed to differences in mTORC1 activity. Activated Akt can phosphorylate and activate mTOR or inhibit PRAS40, an endogenous mTORC1 inhibitor.[7] The AMPK pathway leads to inhibition of mTORC1.[17] However, at least part of the effect of cholesterol-lowering gene therapy on p-mTOR is independent of Akt and AMPK because no effect on Akt and AMPK was observed in the absence of pressure overload.

The reappearance of a fetal metabolic pattern characterized by decreased fatty acid oxidation, increased glycolysis, and increased anaplerosis has been repeatedly demonstrated in models of pathological hypertrophy.[18–22] Cholesterol lowering had a profound effect on metabolic remodeling induced by pressure overload. Glucose uptake in the myocardium was strikingly lower in AAV8-LDLr TAC mice compared with control TAC mice. Although this does not obligatory imply a difference in glucose oxidation, several lines of evidence suggest that cholesterol lowering interfered with a switch of fatty acids to glucose as metabolic substrate in mice with pressure overload. First of all, cholesterol-lowering gene therapy in TAC mice decreased myocardial protein levels of PDH, which catalyzes oxidative decarboxylation of pyruvate to form acetyl-CoA and increased protein levels of PDHK, which inactivates PDH. These data suggest that changes in glucose oxidation may parallel shifts in glucose uptake. Second, data on myocardial ACC protein levels and on p-AAC protein levels, representing the inactive form of the enzyme, suggest lower activity of this enzyme following cholesterol-lowering gene transfer. Because malonyl-CoA production via ACC inhibits fatty acid transport across the mitochondrial membrane via carnitine palmitoyl transferase I,[23] reduced ACC activity following cholesterol lowering would maintain fatty acid oxidation. Finally, the potent effect of cholesterol lowering on fatty acid oxidation in TAC mice is indicated by the significantly increased PPAR-α levels in AAV8-LDLr TAC mice compared with control TAC mice. PPAR-α is a key transcriptional factor regulating substrate metabolism that induces CPT1B expression[24] and expression of PDHK.[25]

The question of whether the metabolic phenotype is the cause or consequence of cardiac dysfunction has been debated. Cardiac-specific deletion of ACC 2, which induced a significant reduction of cardiac malonyl-CoA levels and led to a maintenance of fatty acid oxidation, attenuated cardiac hypertrophy and significantly reduced cardiac fibrosis following pressure overload.[22] Therefore, the observations on ACC may be of particular importance to understand the

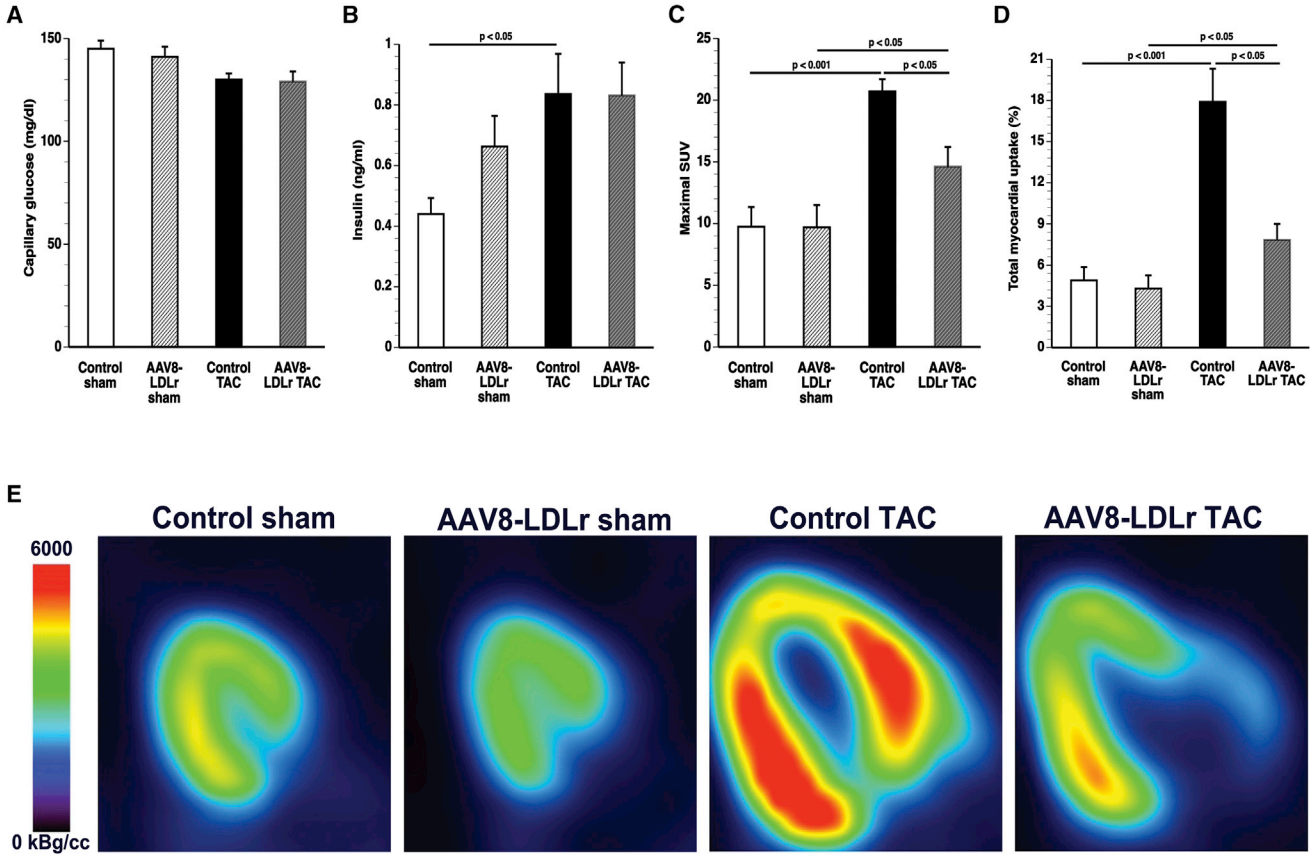

Figure 5. Cholesterol-Lowering Gene Transfer Counteracts Metabolic Remodeling

(A and B) Capillary glucose (A) and plasma insulin levels (B) in control sham (n = 10), AAV8-LDLr sham (n = 10), control TAC (n = 11), and AAV8-LDLr TAC (n = 11) mice 8 weeks after operation. (C and D) Quantification of glucose uptake in the myocardium determined by micro-PET as shown by the maximal standardized uptake (SUV) value (C) and total myocardial uptake (% of injected dose) (D) 8 weeks after sham operation or after TAC (n = 10 in each group). (E) Representative micro-PET images illustrating the uptake of [^{18}F]-FDG in the myocardium of sham mice and TAC mice at day 56 after operation. Error bars represent SEM.

effect of cholesterol lowering on cardiac structure and function. The observed effects of cholesterol lowering on ACC protein levels may reflect differences in p-mTOR levels. Sterol regulatory element binding protein (SREBP-1) activation may be regulated via mTORC-1,[26,27] and the mTOR inhibitor rapamycin has been shown to reduce the expression of many SREBP-1 target genes, including ACC.[28]

MicroRNAs play an important role in regulating lipoprotein metabolism,[29] and these microRNAs also contribute to the regulation of fatty acid metabolism.[30] The effect of plasma cholesterol levels on several microRNAs has been demonstrated.[31] In the current study, we are forcing the system by drastically reducing plasma cholesterol levels via AAV8-mediated LDLr expression in hepatocytes. AAV8-mediated LDLr expression is expected to affect the levels of several microRNAs and may therefore affect mRNA stability or translation of transcription factors and enzymes involved in substrate metabolism. This may explain why the predominant effect in our experiments is at the level of protein expression and not, e.g., at the level of the degree of phosphorylation in case of proteins that are activated by phosphorylation.

The current study was designed as a prevention study because cholesterol-lowering gene therapy was performed before TAC. Therefore, the study is not the equivalent of a clinical intervention study in patients with established heart failure. The prevention study design allowed us to demonstrate a potent effect of cholesterol-lowering gene therapy on mortality after TAC but represents at the same time a limitation of the current study. Whether cholesterol-lowering gene therapy improves established heart failure remains to be established.

In conclusion, cholesterol-lowering gene therapy in mice improves survival, attenuates left ventricular hypertrophy, mitigates metabolic remodeling, and enhances cardiac function in a model of pressure-overload-induced cardiomyopathy. The effect of cholesterol lowering on p-mTOR and ACC may be a critical mediator of the observed beneficial effects. The profound impact of plasma

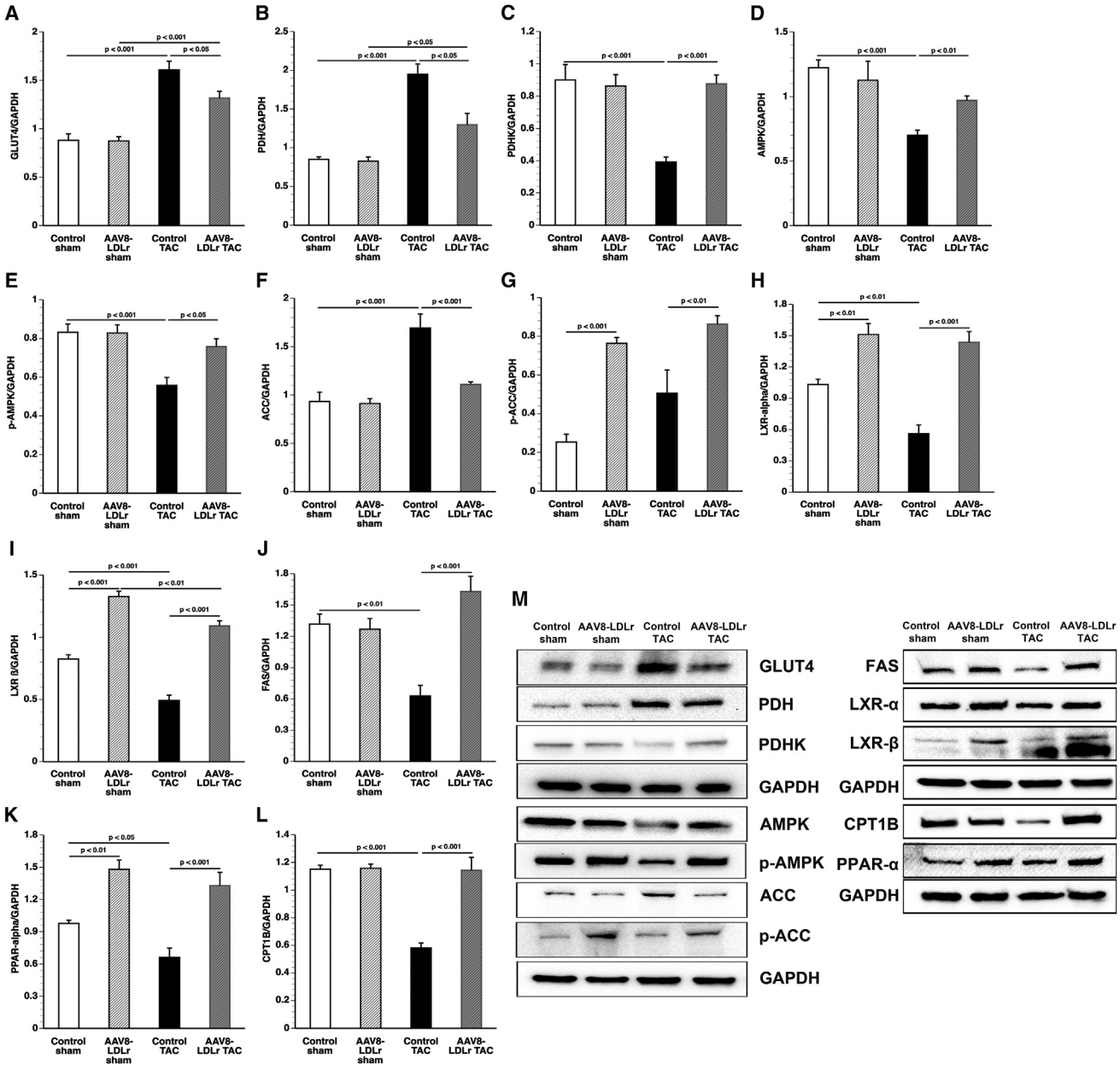

Figure 6. Quantification of Metabolic Proteins by Western Blot

(A–L) Bar graphs illustrating GLUT4 (A), PDH (B), PDHK (C), AMPK (D), p-AMPK (E), AAC (F), p-ACC (G), PPAR-α (H), CPT1B (I), LXR-α (J), LXR-β (K), and FAS (L) protein levels quantified by western blot in the myocardium of control sham (n = 10), AAV8-LDLr sham (n = 10), control TAC (n = 9), and AAV8-LDLr TAC (n = 10) mice 8 weeks after operation. All protein levels were normalized to the glyceraldehyde-3-phosphate dehydrogenase (GAPDH) protein level. (M) Representative images of western blots are shown. Error bars represent SEM.

cholesterol on myocardial biology suggests that targeted cholesterol-lowering therapies may be beneficial for prevention of heart failure.

MATERIALS AND METHODS

For detailed methodology, see the Supplemental Materials and Methods.

Construction, Generation, and Production of Gene Transfer Vectors

Cholesterol-lowering gene therapy was performed using an adeno-associated viral (AAV) serotype 8 vector containing a hepatocyte-specific expression cassette[32] to induce expression of the murine LDLr (AAV8-LDLr). The expression cassette of this vector consists of the 1,272 bp *DC172* promoter, comprising an 890 bp *α1-antitrypsin*

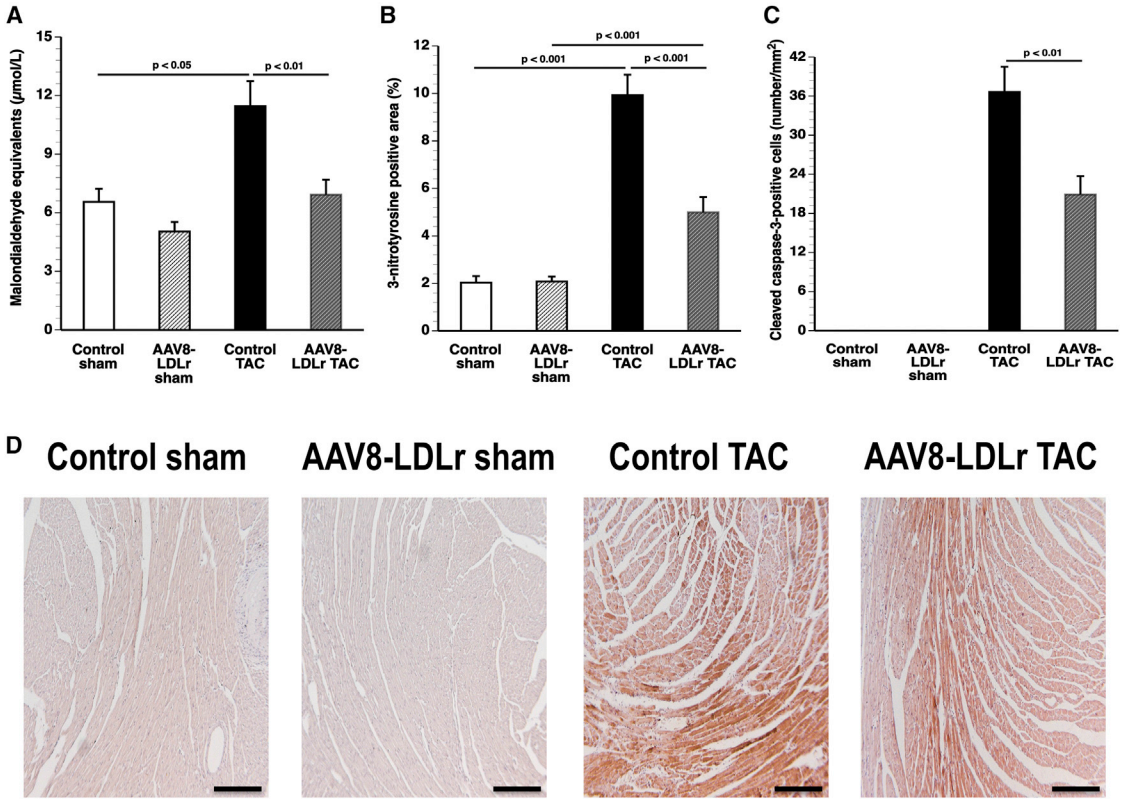

Figure 7. Oxidative Stress and Myocardial Apoptosis Are Reduced by Cholesterol-Lowering Gene Transfer in Mice with Chronic Pressure Overload

(A–C) Bar graphs illustrating plasma TBARSs expressed as plasma malondialdehyde equivalents (A), the percentage of 3-nitrotyrosine-positive area in the myocardium (B), and the number of cleaved caspase-3-positive cells (C) in control sham (n = 15), AAV8-LDLr sham (n = 22), control TAC (n = 23), and AAV8-LDLr TAC (n = 23) mice 8 weeks after operation. (D) Representative photomicrographs showing myocardial sections stained for 3-nitrotyrosine. Scale bars, 100 μm. Error bars represent SEM.

promoter fused together with two copies of the 160 bp α_1-*microglobulin* enhancer,[32] upstream of the human *A-I 5′UTR* containing the first intron (247 bp) followed by the murine *LDLr* cDNA sequence (2,598 bp), one copy of the 774 bp *hepatic control region-1*, and the rabbit β-globin polyadenylation signal (127 bp). AAV vector production was performed as described previously.[33]

In Vivo Experiments on the Effect of Cholesterol-Lowering Gene Therapy on Cardiac Remodeling

All experimental procedures in animals were performed in accordance with protocols approved by the Institutional Animal Care and Research Advisory Committee of the Catholic University of Leuven (approval no. P154/2013). At the age of 12 weeks, female C57BL/6 LDLr$^{-/-}$ mice, originally purchased from Jackson Laboratories, were fed standard chow diet (Sniff Spezialdiäten) supplemented with 0.2% cholesterol 10% coconut oil to induce pronounced hypercholesterolemia. Gene transfer in C57BL/6 LDLr$^{-/-}$ mice was performed at the age of 15 weeks by tail-vein injection of 2×10^{12} genome copies/kg AAV8-LDLr. Control mice were untreated. To induce pressure overload, we performed TAC 2 weeks later.[34,35] TAC initially leads to compensatory hypertrophy of the heart, but over time the response to chronic hemodynamic overload becomes maladaptive and results in cardiac dilatation and heart failure. The sham procedure was identical except that no constriction on the aorta was applied. Anesthesia was performed with a single intraperitoneal injection of sodium pentobarbital (Nembutal; Ceva Sante Animale) at a dose of 40–70 mg/kg. All randomized mice were included in the analyses. Morphometric and hemodynamic quantifications were performed in a blinded fashion.

In Vivo Hemodynamic Measurements

Invasive hemodynamic measurements were performed 8 weeks after TAC or after sham operation as described previously.[36] Mice were anesthetized by intraperitoneal administration of 1.4 g/kg urethane (Sigma).

Evaluation of Cardiac Glucose Metabolism by Micro-PET

Glucose uptake in the myocardium and in the skeletal muscle was quantified by micro-PET using [^{18}F]-fluorodeoxyglucose (FDG) as a tracer (309 ± 22 μCi). Imaging was performed 60 min after tracer administration. Animals were anesthetized by inhalation of 2% isoflurane in 100% oxygen and underwent static imaging for 10 min on a micro-PET Focus 220 scanner (Concorde Microsystems). Images were reconstructed with ordered subset expectation

maximization algorithm with six iterations (OSEM3D 6i) and analyzed with PMOD v.3.4 (Pmod Technologies).

Statistical Analysis

All data are expressed as means ± SEM. Parameters between four groups were compared by one-way analysis of variance followed by Bonferroni multiple comparisons post-test for comparing sham groups, TAC groups, and sham versus respective TAC groups using GraphPad Instat (GraphPad Software). When indicated, a logarithmic transformation or a square root transformation or a non-parametric test was performed. Parameters between two groups were compared using Student's t test. When indicated, a logarithmic transformation, a square root transformation, or a non-parametric Mann-Whitney test was performed. The assumption of Gaussian distribution was tested using the Kolmogorov and Smirnov method. Kaplan-Meier survival curves were analyzed by log rank test using Prism4 (GraphPad Software). A two-sided p value of less than 0.05 was considered statistically significant.

SUPPLEMENTAL INFORMATION

Supplemental Information includes Supplemental Materials and Methods, six figures, and four tables and can be found with this article online at http://dx.doi.org/10.1016/j.ymthe.2017.07.017.

AUTHOR CONTRIBUTIONS

Conceptualization, I.M., B.D.G.; Methodology, I.M., A.P., T.D., U.H., P.P.V.V., O.G., F.J.; Formal Analysis, I.M., A.P., T.D., P.P.V.V., B.D.G.; Investigation, I.M., R.A., M.M., J.P.A.; Writing – Original Draft, I.M., B.D.G.; Writing – Review & Editing, R.A., M.M., J.P.A., T.D., U.H., P.P.V.V., O.G., F.J.; Funding Acquisition, B.D.G.

CONFLICTS OF INTEREST

The authors declare no conflict of interest.

ACKNOWLEDGMENTS

I.M. is a postdoctoral fellow of the Fonds voor Wetenschappelijk Onderzoek-Vlaanderen. This work was supported by Onderzoekstoelagen grant OT/13/090 of the KU Leuven and grant G0A3114N of the Fonds voor Wetenschappelijk Onderzoek-Vlaanderen.

REFERENCES

1. Velagaleti, R.S., Massaro, J., Vasan, R.S., Robins, S.J., Kannel, W.B., and Levy, D. (2009). Relations of lipid concentrations to heart failure incidence: the Framingham Heart Study. Circulation *120*, 2345–2351.
2. Kjekshus, J., Apetrei, E., Barrios, V., Böhm, M., Cleland, J.G., Cornel, J.H., Dunselman, P., Fonseca, C., Goudev, A., Grande, P., et al.; CORONA Group (2007). Rosuvastatin in older patients with systolic heart failure. N. Engl. J. Med. *357*, 2248–2261.
3. Tavazzi, L., Maggioni, A.P., Marchioli, R., Barlera, S., Franzosi, M.G., Latini, R., Lucci, D., Nicolosi, G.L., Porcu, M., and Tognoni, G.; Gissi-HF Investigators (2008). Effect of rosuvastatin in patients with chronic heart failure (the GISSI-HF trial): a randomised, double-blind, placebo-controlled trial. Lancet *372*, 1231–1239.
4. Felker, G.M. (2010). Coenzyme Q10 and statins in heart failure: the dog that didn't bark. J. Am. Coll. Cardiol. *56*, 1205–1206.
5. Moosmann, B., and Behl, C. (2004). Selenoprotein synthesis and side-effects of statins. Lancet *363*, 892–894.
6. Glazer, H.P., Osipov, R.M., Clements, R.T., Sellke, F.W., and Bianchi, C. (2009). Hypercholesterolemia is associated with hyperactive cardiac mTORC1 and mTORC2 signaling. Cell Cycle *8*, 1738–1746.
7. Sciarretta, S., Volpe, M., and Sadoshima, J. (2014). Mammalian target of rapamycin signaling in cardiac physiology and disease. Circ. Res. *114*, 549–564.
8. Zhu, Y., Soto, J., Anderson, B., Riehle, C., Zhang, Y.C., Wende, A.R., Jones, D., McClain, D.A., and Abel, E.D. (2013). Regulation of fatty acid metabolism by mTOR in adult murine hearts occurs independently of changes in PGC-1α. Am. J. Physiol. Heart Circ. Physiol. *305*, H41–H51.
9. Cesselli, D., Jakoniuk, I., Barlucchi, L., Beltrami, A.P., Hintze, T.H., Nadal-Ginard, B., Kajstura, J., Leri, A., and Anversa, P. (2001). Oxidative stress-mediated cardiac cell death is a major determinant of ventricular dysfunction and failure in dog dilated cardiomyopathy. Circ. Res. *89*, 279–286.
10. Molyneux, S.L., Florkowski, C.M., George, P.M., Pilbrow, A.P., Frampton, C.M., Lever, M., and Richards, A.M. (2008). Coenzyme Q10: an independent predictor of mortality in chronic heart failure. J. Am. Coll. Cardiol. *52*, 1435–1441.
11. Loscalzo, J. (2014). Keshan disease, selenium deficiency, and the selenoproteome. N. Engl. J. Med. *370*, 1756–1760.
12. Xu, J., Dang, Y., Ren, Y.R., and Liu, J.O. (2010). Cholesterol trafficking is required for mTOR activation in endothelial cells. Proc. Natl. Acad. Sci. USA *107*, 4764–4769.
13. Shioi, T., McMullen, J.R., Tarnavski, O., Converso, K., Sherwood, M.C., Manning, W.J., and Izumo, S. (2003). Rapamycin attenuates load-induced cardiac hypertrophy in mice. Circulation *107*, 1664–1670.
14. McMullen, J.R., Sherwood, M.C., Tarnavski, O., Zhang, L., Dorfman, A.L., Shioi, T., and Izumo, S. (2004). Inhibition of mTOR signaling with rapamycin regresses established cardiac hypertrophy induced by pressure overload. Circulation *109*, 3050–3055.
15. Völkers, M., Toko, H., Doroudgar, S., Din, S., Quijada, P., Joyo, A.Y., Ornelas, L., Joyo, E., Thuerauf, D.J., Konstandin, M.H., et al. (2013). Pathological hypertrophy amelioration by PRAS40-mediated inhibition of mTORC1. Proc. Natl. Acad. Sci. USA *110*, 12661–12666.
16. Wang, X., Li, L., Niu, X., Dang, X., Li, P., Qu, L., Bi, X., Gao, Y., Hu, Y., Li, M., et al. (2014). mTOR enhances foam cell formation by suppressing the autophagy pathway. DNA Cell Biol. *33*, 198–204.
17. Inoki, K., Ouyang, H., Zhu, T., Lindvall, C., Wang, Y., Zhang, X., Yang, Q., Bennett, C., Harada, Y., Stankunas, K., et al. (2006). TSC2 integrates Wnt and energy signals via a coordinated phosphorylation by AMPK and GSK3 to regulate cell growth. Cell *126*, 955–968.
18. Akki, A., Smith, K., and Seymour, A.M. (2008). Compensated cardiac hypertrophy is characterised by a decline in palmitate oxidation. Mol. Cell. Biochem. *311*, 215–224.
19. Nascimben, L., Ingwall, J.S., Lorell, B.H., Pinz, I., Schultz, V., Tornheim, K., and Tian, R. (2004). Mechanisms for increased glycolysis in the hypertrophied rat heart. Hypertension *44*, 662–667.
20. Sorokina, N., O'Donnell, J.M., McKinney, R.D., Pound, K.M., Woldegiorgis, G., LaNoue, K.F., Ballal, K., Taegtmeyer, H., Buttrick, P.M., and Lewandowski, E.D. (2007). Recruitment of compensatory pathways to sustain oxidative flux with reduced carnitine palmitoyltransferase I activity characterizes inefficiency in energy metabolism in hypertrophied hearts. Circulation *115*, 2033–2041.
21. Pound, K.M., Sorokina, N., Ballal, K., Berkich, D.A., Fasano, M., Lanoue, K.F., Taegtmeyer, H., O'Donnell, J.M., and Lewandowski, E.D. (2009). Substrate-enzyme competition attenuates upregulated anaplerotic flux through malic enzyme in hypertrophied rat heart and restores triacylglyceride content: attenuating upregulated anaplerosis in hypertrophy. Circ. Res. *104*, 805–812.
22. Kolwicz, S.C., Jr., Olson, D.P., Marney, L.C., Garcia-Menendez, L., Synovec, R.E., and Tian, R. (2012). Cardiac-specific deletion of acetyl CoA carboxylase 2 prevents metabolic remodeling during pressure-overload hypertrophy. Circ. Res. *111*, 728–738.
23. Saddik, M., Gamble, J., Witters, L.A., and Lopaschuk, G.D. (1993). Acetyl-CoA carboxylase regulation of fatty acid oxidation in the heart. J. Biol. Chem. *268*, 25836–25845.
24. Mascaró, C., Acosta, E., Ortiz, J.A., Marrero, P.F., Hegardt, F.G., and Haro, D. (1998). Control of human muscle-type carnitine palmitoyltransferase I gene transcription by peroxisome proliferator-activated receptor. J. Biol. Chem. *273*, 8560–8563.

25. Huang, B., Wu, P., Bowker-Kinley, M.M., and Harris, R.A. (2002). Regulation of pyruvate dehydrogenase kinase expression by peroxisome proliferator-activated receptor-alpha ligands, glucocorticoids, and insulin. Diabetes *51*, 276–283.

26. Porstmann, T., Santos, C.R., Griffiths, B., Cully, M., Wu, M., Leevers, S., Griffiths, J.R., Chung, Y.L., and Schulze, A. (2008). SREBP activity is regulated by mTORC1 and contributes to Akt-dependent cell growth. Cell Metab. *8*, 224–236.

27. Laplante, M., and Sabatini, D.M. (2009). An emerging role of mTOR in lipid biosynthesis. Curr. Biol. *19*, R1046–R1052.

28. Brown, N.F., Stefanovic-Racic, M., Sipula, I.J., and Perdomo, G. (2007). The mammalian target of rapamycin regulates lipid metabolism in primary cultures of rat hepatocytes. Metabolism *56*, 1500–1507.

29. Aryal, B., Singh, A.K., Rotllan, N., Price, N., and Fernández-Hernando, C. (2017). MicroRNAs and lipid metabolism. Curr. Opin. Lipidol. *28*, 273–280.

30. Dávalos, A., Goedeke, L., Smibert, P., Ramírez, C.M., Warrier, N.P., Andreo, U., Cirera-Salinas, D., Rayner, K., Suresh, U., Pastor-Pareja, J.C., et al. (2011). miR-33a/b contribute to the regulation of fatty acid metabolism and insulin signaling. Proc. Natl. Acad. Sci. USA *108*, 9232–9237.

31. Desgagné, V., Bouchard, L., and Guérin, R. (2017). microRNAs in lipoprotein and lipid metabolism: from biological function to clinical application. Clin. Chem. Lab. Med. *55*, 667–686.

32. Jacobs, F., Snoeys, J., Feng, Y., Van Craeyveld, E., Lievens, J., Armentano, D., Cheng, S.H., and De Geest, B. (2008). Direct comparison of hepatocyte-specific expression cassettes following adenoviral and nonviral hydrodynamic gene transfer. Gene Ther. *15*, 594–603.

33. Lock, M., Alvira, M., Vandenberghe, L.H., Samanta, A., Toelen, J., Debyser, Z., and Wilson, J.M. (2010). Rapid, simple, and versatile manufacturing of recombinant adeno-associated viral vectors at scale. Hum. Gene Ther. *21*, 1259–1271.

34. Buys, E.S., Raher, M.J., Blake, S.L., Neilan, T.G., Graveline, A.R., Passeri, J.J., Llano, M., Perez-Sanz, T.M., Ichinose, F., Janssens, S., et al. (2007). Cardiomyocyte-restricted restoration of nitric oxide synthase 3 attenuates left ventricular remodeling after chronic pressure overload. Am. J. Physiol. Heart Circ. Physiol. *293*, H620–H627.

35. Hu, P., Zhang, D., Swenson, L., Chakrabarti, G., Abel, E.D., and Litwin, S.E. (2003). Minimally invasive aortic banding in mice: effects of altered cardiomyocyte insulin signaling during pressure overload. Am. J. Physiol. Heart Circ. Physiol. *285*, H1261–H1269.

36. Muthuramu, I., Singh, N., Amin, R., Nefyodova, E., Debasse, M., Van Horenbeeck, I., Jacobs, F., and De Geest, B. (2015). Selective homocysteine-lowering gene transfer attenuates pressure overload-induced cardiomyopathy via reduced oxidative stress. J. Mol. Med. (Berl.) *93*, 609–618.

YMTHE, Volume *25*

Supplemental Information

Cholesterol-Lowering Gene Therapy Counteracts the Development of Non-ischemic Cardiomyopathy in Mice

Ilayaraja Muthuramu, Ruhul Amin, Andrey Postnov, Mudit Mishra, Joseph Pierre Aboumsallem, Tom Dresselaers, Uwe Himmelreich, Paul P. Van Veldhoven, Olivier Gheysens, Frank Jacobs, and Bart De Geest

SUPPLEMENTAL FIGURES

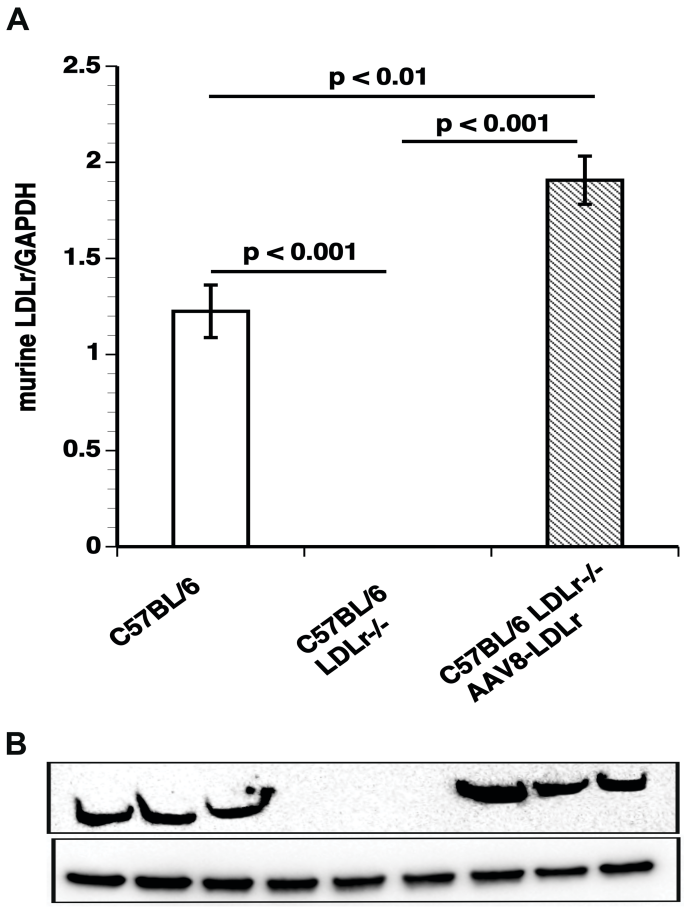

Figure S1. Murine LDLr expression in the liver. Bar graph (A) illustrating murine LDLr protein levels quantified by western blot in the liver of C57BL/6 mice (n=6), of C57BL/6 LDLr$^{-/-}$ mice (n=6), and of C57BL/6 LDLr$^{-/-}$ mice (n=6) 10 weeks after gene transfer with 2 x 10^{12} genome copies/kg of AAV8-LDLr. All protein levels were normalized to the glyceraldehyde-3-phosphate dehydrogenase (GAPDH) protein level. Representative images of western blots are shown in panel B. The first three lanes correspond to C57BL/6 mice, the next three lanes illustrate C57BL/6 LDLr$^{-/-}$ mice, and the final three lanes correspond to AAV8-LDLr-treated C57BL/6 LDLr$^{-/-}$ mice. Error bars represent SEM.

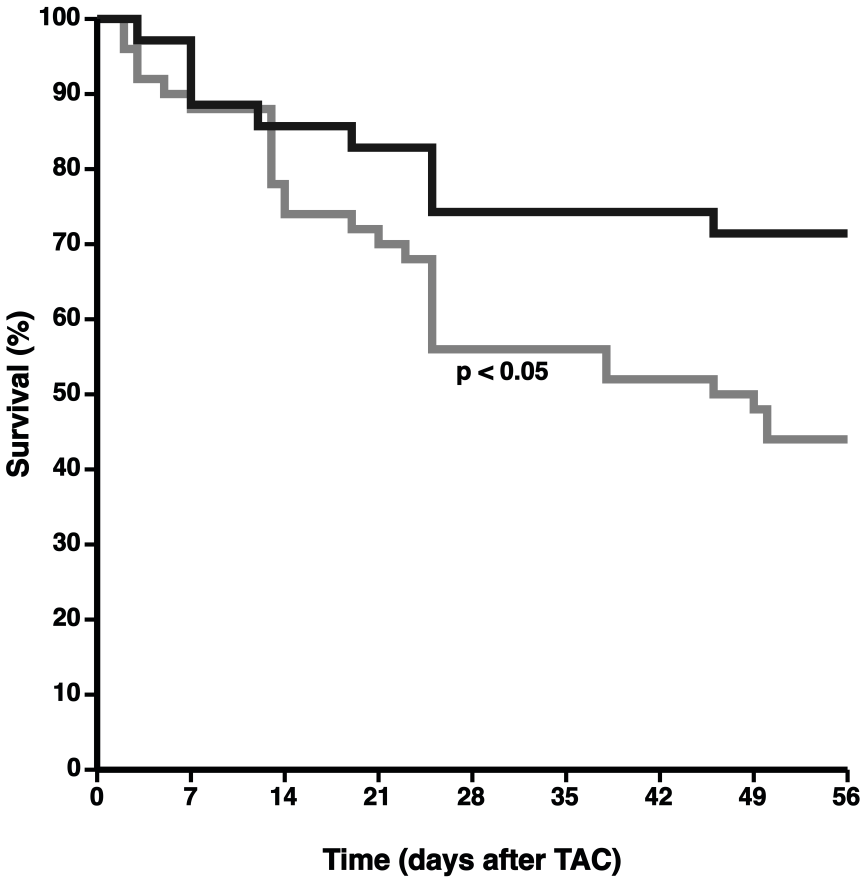

Figure S2. Comparison of Kaplan-Meier survival curves during an 8 weeks follow-up period after TAC. Control TAC mice (grey line) and AAV8-LDLr TAC mice (black line) are compared. The 0 day time-point corresponds to the induction of TAC at the age of 17 weeks. Survival analysis was performed by log-rank test.

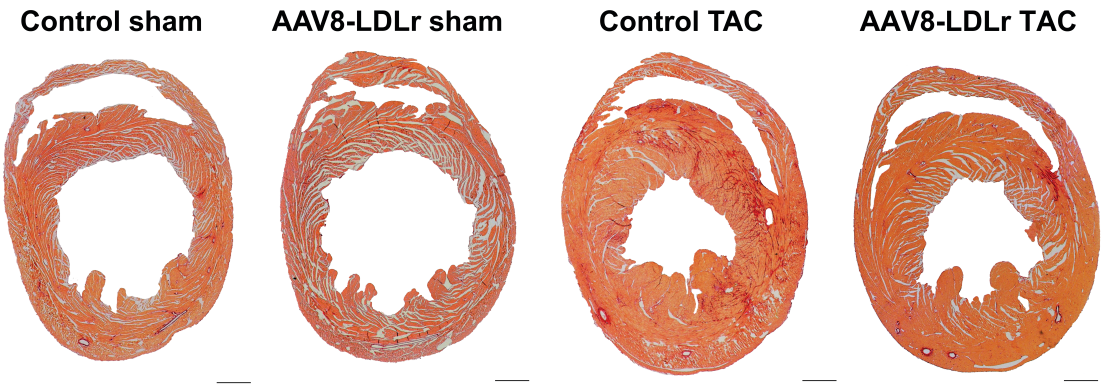

Figure S3. Representative Sirius red stained cross-sections of sham hearts and TAC hearts at day 56 after operation. Scale bar represents 1 mm.

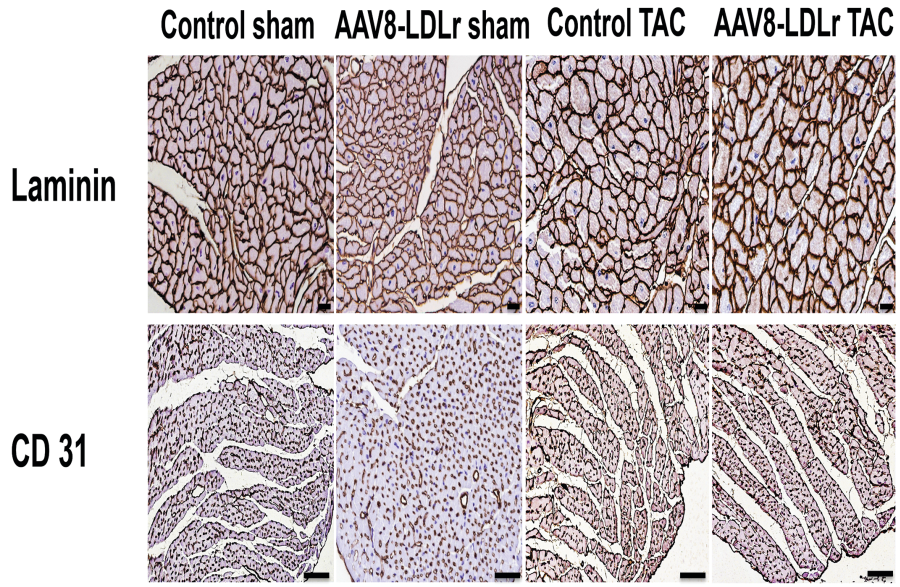

Figure S4. Immunohistochemical analysis of the myocardium of sham mice and TAC mice at day 56 after operation. Representative photomicrographs show laminin-stained cardiomyocytes and CD31-positive capillaries. Scale bar represents 50 μm.

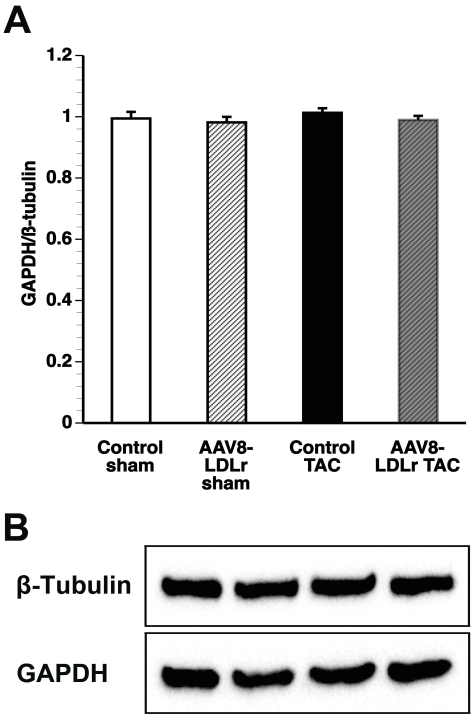

Figure S5. GAPDH is an adequate reference for normalizing protein expression levels. Bar graph (A) illustrating the GAPDH/ß-tubulin protein level ratio in the myocardium of control sham (n=10), AAV8-LDLr sham (n=10), control TAC (n=9), and AAV8-LDLr TAC (n=10) mice 8 weeks after operation. Representative images of western blots are shown in panel B. Error bars represent SEM.

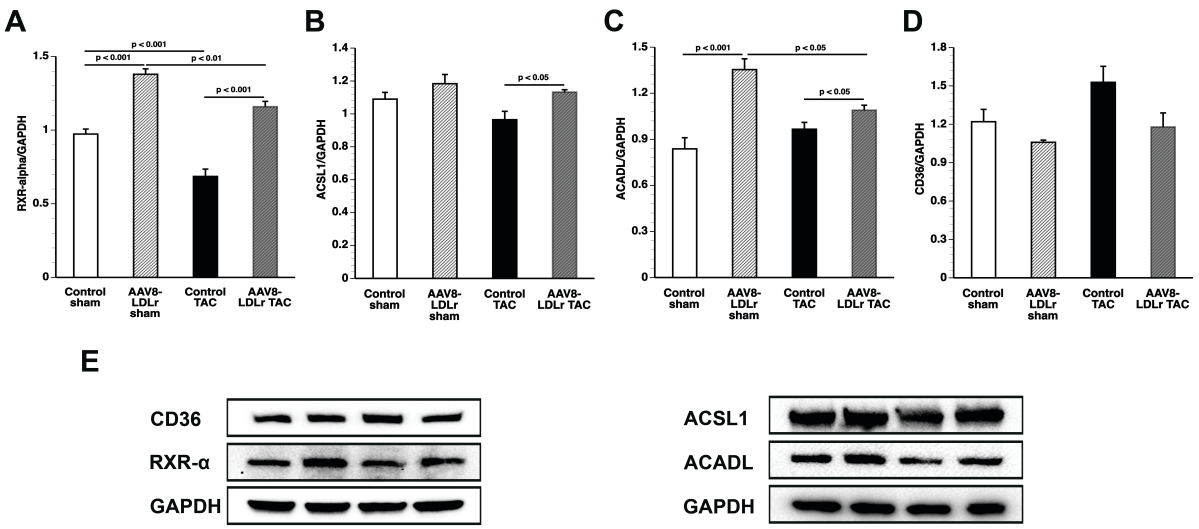

Figure S6. Quantification of RXR-α and of metabolic proteins by western blot. Bar graphs illustrating RXR-α (A), ACSL1 (B), ACADL (C), and CD36 (D) protein levels quantified by western blot in the myocardium of control sham (n=10), AAV8-LDLr sham (n=10), control TAC (n=9), and AAV8-LDLr TAC (n=10) mice 8 weeks after operation. All protein levels were normalized to the GAPDH protein level. Representative images of western blots are shown in panel E. Error bars represent SEM.

SUPPLEMENTAL TABLES

Table S1. Total and non-HDL, VLDL, IDL, LDL and HDL plasma cholesterol (mmol/L) at day 10 after gene transfer with 2 x 10^{12} genome copies/kg of AAV8-LDLr in female C57BL/6 LDLr$^{-/-}$ mice compared to control female C57BL/6 LDLr$^{-/-}$ mice.

	Controls	AAV8-LDLr
Total	9.26 ± 0.39	1.59 ± 0.08****
Non-HDL	7.89 ± 0.36	0.714 ± 0.039****
VLDL	1.75 ± 0.10	0.160 ± 0.010****
IDL	3.57 ± 0.31	0.235 ± 0.013****
LDL	2.57 ± 0.12	0.318 ± 0.018****
HDL	1.37 ± 0.07	0.879 ± 0.054***

Data are expressed as means ± S.E.M. (n=6 for each condition). Lipoproteins were isolated by ultracentrifugation. ***: $p<0.001$; ****: $p<0.0001$ for comparison versus controls.

Table S2. Myocardial lipid levels 8 weeks after sham operation or after TAC.

	Control sham	AAV8-LDLr sham	Control TAC	AAV8-LDLr TAC
Number of mice	10	10	9	11
Phospholipids (nmol/mg tissue)	51.6 ± 0.9	52.0 ± 1.2	45.9 ± 0.9§§	48.2 ± 1.1
Cholesterol (pmol/nmol phospholipids)	75.4 ± 1.7	73.7 ± 2.4	82.5 ± 3.9	77.0 ± 3.7
Cholesteryl esters (pmol/nmol phospholipids)	16.3 ± 2.4	8.79 ± 3.11°	20.6 ± 5.6	4.87 ± 0.56**
Triglycerides (pmol/nmol phospholipids)	68.4 ± 4.9	52.8 ± 3.6°	43.4 ± 2.3§§	56.9 ± 6.8
Free fatty acids (pmol/nmol phospholipids)	4.45 ± 1.53	12.4 ± 4.3	11.5 ± 1.5§	11.8 ± 1.8
Sphingomyelin (pmol/nmol phospholipids)	24.9 ± 2.0	27.3 ± 3.6	34.3 ± 1.9§	32.5 ± 2.2

Sham operation or TAC was performed at the age of 17 weeks.
Data are expressed as means ± SEM. °: $p<0.05$ versus control sham. §: $p<0.05$; §§**:** $p<0.01$ versus respective sham groups.**: $p<0.01$ versus control TAC.

Table S3. Morphometric and histological parameters of the left ventricular myocardium 8 weeks after sham operation and after TAC in C57BL/6 LDLr$^{-/-}$ mice.

Sham operation or TAC was performed at the age of 17 weeks.

	Control sham	AAV8-LDLr sham	Control TAC	AAV8-LDLr TAC
Number of mice	15	22	23	23
LV wall area (mm^2)	9.06 ± 0.17	8.67 ± 0.17	12.4 ± 0.4§§§	10.6 ± 0.4§§§***
Septal wall thickness (µm)	1070 ± 14	1060 ± 20	1320 ± 40§§§	1230 ± 30§§
Anterior wall thickness (µm)	1100 ± 10	1120 ± 20	1370 ± 30§§§	1300 ± 40§
Cardiomyocyte cross-sectional (μm^2)	230 ± 17	187 ± 6$^{°}$	480 ± 20§§§	410 ± 20§§§*
Cardiomyocyte density (number/mm^2)	4520 ± 280	5630 ± 170$^{°°°}$	3050 ± 120§§§	3480 ± 170§§§
Capillary density (number/mm^2)	6040 ± 340	7310 ± 220$^{°}$	4480 ± 240§§§	4360 ± 170§§§
Relative vascularity (μm^{-2})	0.00617 ± 0.00041	0.00716 ± 0.00027$^{°}$	0.00315 ± 0.00016§§§	0.00319 ± 0.00013§§§

Data are expressed as means ± SEM. °: p<0.05;°°°: p<0.001 versus control sham. §: p<0.05; §§: p<0.01; §§§: p<0.001 versus respective sham groups. *: p<0.05; ***: p<0.001 versus control TAC.

Table S4. Quantification of glucose uptake in the myocardium determined by micro-PET parameters 8 weeks after sham operation or after TAC in C57BL/6 LDLr$^{-/-}$ mice.

	Control sham	AAV8-LDLr sham	Control TAC	AAV8-LDLr TAC
Number of mice	10	10	11	11
Maximal SUV	9.75 ± 1.58	9.69 ± 1.80	20.7 ± 1.0§§§	14.6 ± 1.6§*
SUV 50%	6.99 ± 1.17	6.89 ± 1.32	13.9 ± 0.8§§§	10.0 ± 1.1§§*
Volume 50% (mm^3)	103 ± 7	96.5 ± 3.1	143 ± 17§	97.8 ± 5.5**
SUV 75%	8.25 ± 1.35	8.16 ± 1.53	17.2 ± 0.9§§§	12.2 ± 1.3§*
Volume 75% (mm^3)	40.5 ± 3.0	35.1 ± 2.4	36.4 ± 6.0	29.3 ± 3.6
Total myocardial uptake (%)	4.90 ± 0.96	4.29 ± 0.96	17.9 ± 2.4§§§	7.84 ± 1.16§*
SUV left quadriceps	0.375 ± 0.054	0.381 ± 0.045	0.318 ± 0.056	0.402 ± 0.067

Sham operation or TAC was performed at the age of 17 weeks. Micro-PET analysis was performed at the age of 25 weeks.
SUV: standardized uptake value. SUV 50%: average SUV in voxels with a value above 50% of the maximal SUV. SUV 75%: average SUV in voxels with a value above 75% of the maximal SUV.
Volume 50%: integrated volume of voxels with a value above 50% of the maximal SUV. Volume 75%: integrated volume of voxels with a value above 75% of the maximal SUV.
Data are expressed as means ± SEM. §: $p<0.05$; §§§: $p<0.001$ versus respective Sham groups; *: $p<0.05$; **: $p<0.01$ versus Control TAC.

SUPPLEMENTAL MATERIALS AND METHODS

Construction, generation, and production of gene transfer vectors-Cholesterol lowering gene therapy was performed using an AAV8 vector containing a hepatocyte-specific expression cassette to induce expression of the murine low-density lipoprotein receptor (LDLr) (AAV8-LDLr). The expression cassette of this vector consists of the 1272 bp *DC172* promoter, comprising an 890 bp α_1*-antitrypsin* promoter fused together with 2 copies of the 160 bp α_1*-microglobulin* enhancer[1], upstream of the human *A-I 5'UTR* containing the first intron (247 bp) followed by the murine *LDLr* cDNA sequence (2598 bp), and the rabbit ß-globin polyadenylation signal (127 bp). The transcriptional regulatory sequences in this expression cassette are hepatocyte-specific[1]. AAV vector production was performed as described[2].

In vivo experiments on the effect of cholesterol lowering gene therapy on cardiac remodeling-All experimental procedures in animals were performed in accordance with protocols approved by the Institutional Animal Care and Research Advisory Committee of the Catholic University of Leuven (Approval number: P154/2013). At the age of 12 weeks, female C57BL/6 LDLr$^{-/-}$ mice, originally purchased from Jackson Laboratories (Bar Harbor, ME, USA), were fed standard chow diet (Sniff Spezialdiäten GMBH, Soest, Germany) supplemented with 0.2% cholesterol 10% coconut oil to induce pronounced hypercholesterolemia. Gene transfer in C57BL/6 LDLr$^{-/-}$ mice was performed at the age of 15 weeks by tail vein injection of 2 x 10^{12} genome copies/kg of AAV8-LDLr. Control mice were untreated. To induce pressure overload, TAC was performed two weeks later[3, 4]. Briefly, anesthesia was performed with a single intraperitoneal injection of sodium pentobarbital (Nembutal®, Ceva Sante Animale, Brussels, Belgium) at a dose of 40-70 mg/kg. Mice were put in supine position and temperature was maintained at 37°C with a heating pad. A horizontal skin incision of 0.5 cm to 1 cm in length was made at the level of the suprasternal notch. A 2 mm to 3 mm longitudinal cut was performed in the proximal portion of the sternum and the thymus gland was retracted. This allowed visualization of the aortic arch under low-power magnification. A wire with a snare at the end was passed under the aorta between the origin of the right innominate artery and the left common carotid artery. A 7-0 silk suture (Ethicon, Johnson & Johnson, Livingston, Scotland) was snared with the wire and pulled back around the aorta. Subsequently, a bent 27-gauge needle (BD Microlance®, BD, Franklin Lakes, New Jersey) was placed next to the aortic arch and the suture was snugly tied around the needle and the aorta. Afterwards, the needle was quickly removed. The skin was closed and mice were allowed to recover on a warming pad until they were fully awake. The sham procedure was identical except that no constriction on the aorta was applied.

In vivo hemodynamic measurements-Invasive hemodynamic measurements were performed 8 weeks after TAC or after sham operation. Mice were anesthetized by intraperitoneal administration of 1.4 g/kg urethane (Sigma, Steinheim, Germany). Body temperature was maintained with a heating pad and monitored with a rectal probe. An incision in the right carotid artery was made with a 26-gauge needle between a distal and proximal non-occlusive ligation of the artery. A 1.0 French Millar pressure catheter (SPR-67/NR; Millar instruments, Houston, Texas, USA) was inserted and advanced to the left ventricle (LV). After stabilisation of the catheter, heart rate, maximal systolic LV pressure, minimal diastolic LV pressure, the peak rate of isovolumetric LV contraction (dP/dt_{max}), and the peak rate of isovolumetric LV relaxation (dP/dt_{min}) were measured. The end-diastolic LV pressure was calculated manually from the pressure in function of time curves. The time constant of isovolumetric LV pressure fall (tau) was calculated using the method of Weiss *et al.*[5]. Arterial blood pressure measurements were obtained after withdrawal of the catheter from the LV to the ascending aorta. Data were registered with Powerlab Bridge Amplifier and Chart Software (sampling rate 2000 Hz; ADInstruments Ltd, Oxford, United Kingdom).

Blood sampling-Blood was collected by puncture of the retro-orbital plexus. Anticoagulation was performed with 0.1 volume of 4% trisodium citrate and plasma was immediately isolated by centrifugation at 1100 g for 10 min and stored at -20°C.

Plasma lipoprotein analysis-Mouse lipoproteins were separated by density gradient ultracentrifugation in a swing-out rotor as described before[6]. Fractions were stored at -20°C until analysis. Non-HDL cholesterol was determined as the sum of cholesterol within very low-density lipoproteins (VLDL) ($0.95 < d < 1.006$ g/ml), intermediate-density lipoproteins (IDL) ($1.006 < d < 1.019$ g/ml), and low-density lipoproteins (LDL) ($1.019 < d < 1.05$ g/ml) lipoprotein fractions. The cut-off value (d=1.05 g/ml) between LDL and high-density lipoproteins (HDL) for murine samples was chosen based on previous work by Camus, Chapman *et al.*[7]. Cholesterol in plasma and lipoprotein fractions was determined with commercially available enzymes (Roche Diagnostics, Basel, Switzerland). Precipath L (Roche Diagnostics) was used as a standard.

Analysis of lipid peroxidation in plasma-Measurement of Thiobarbituric Acid Reactive Substances (TBARS) used for quantification of lipid peroxidation was performed according to the instructions of the manufacturer (Cayman Chemical, Ann Arbor, MI, USA).

Myocardial lipid analysis-Major lipid classes (phospholipids, cholesterol, cholesteryl esters, triglycerides, free fatty acids and sphingomyelin) in the myocardium were analyzed in myocardial lipid extracts with classical (bio)chemical assays[8-11].

Quantification of myocardial protein levels by western blot-Myocardial tissue samples were isolated 56 days after sham operation or TAC and immediately frozen in liquid nitrogen and stored at -80°C. Tissues were placed in lysing matrix tubes (QBiogene/MP Biomedicals, Solon, OH, USA), mixed with 1 ml of protein extraction buffer containing 10 mM imidazole, 300 mM sucrose, 1 mM dithiotreitol, 1mM sodium metabisulfite, 25 mM sodium fluoride, 5 mM sodium ethylenediaminetetraacetic acid, 5 mM sodium pyrophosphate, 0.3 mM phenylmethylsulfonyl fluoride, and a protease inhibitor cocktail (Roche Diagnostics Belgium, Vilvoorde, Belgium)[12], and homogenised in the FastPrep24 instrument (MP Biomedicals). Protein concentration was quantified using the Pierce BCA Protein Assay kit (Pierce Biotechnology Inc., Rockford, IL, USA). Equal amounts of proteins were separated on 4-20 % Tris-Glycine gradient gels (Bio-Rad Laboratories N.V., Temse, Belgium) and blotted onto polyvinylidene difluoride membranes (Bio-Rad Laboratories N.V.). Membranes were incubated with primary antibodies against Akt, phospho (p)-Akt (Ser/Thr), mitogen-activated protein kinase (MAPK) kinase (MEK) 1/2, p-MEK 1/2 (Ser217/221), p38 MAPK, p-p38 MAPK (Thr180/Tyr182), mammalian or mechanistic target of rapamycin (mTOR), p-mTOR (Ser2481), acetyl-coenzyme A (acetyl-CoA) carboxylase (ACC), p-ACC (Ser79), AMP-activated protein kinase (AMPK)α, p-AMPKα (Thr172), c-Jun N-terminal kinase (JNK), also referred to as stress-activated protein kinase (SAPK)/JNK, p-JNK (Thr183/Tyr185), extracellular signal–regulated kinase (ERK) 1/2, p-ERK 1/2 (Thr202/Tyr204), Smad1, p-Smad 1/5 (Ser463/465), Smad4, GLUT 4, pyruvate dehydrogenase (PDH), pyruvate dehydrogenase kinase, transforming growth factor (TGF)-β1, fatty acid synthase (FAS), long-chain acyl-CoA synthetase, member 1 (ACSL1), ß-tubulin, glyceraldehyde 3-phosphate dehydrogenase (GAPDH) (all prior antibodies from Cell Signalling Technologies, Beverly, MA, USA), peroxisome proliferator-activated receptor (PPAR-α), carnitine palmitoyltransferase IB (CPT1B), liver X receptor (LXR)-α and LXR-ß, retinoid X receptor (RXR)-α, fatty acid translocase (CD36), and long-chain acyl-CoA dehydrogenase (ACADL) (Abcam, Cambridge, UK). Protein expression was detected with Super signal west pico chemilumninescent reagents (Thermo Scientific, Rockford, IL, USA) and quantified using Image lab TM Analyzer software (Bio-Rad laboratories N.V.). All protein levels were normalized to the GAPDH protein level.

Quantification of murine LDLr expression in the liver by western blot- Liver tissue samples were isolated and immediately frozen in liquid nitrogen and stored at -80°C. The extraction, blotting, and protein quantification procedures were identical compared to the methodology described for myocardial proteins. The primary antibody for detection of the murine LDLr was obtained from Abcam (Cambrdige, UK).

Histological and morphometric analysis-After hemodynamic analysis, mice were perfused via the abdominal aorta with phosphate-buffered saline (PBS) and hearts were arrested in diastole by $CdCl_2$ (100 µl; 0.1 mol/L), followed by perfusion fixation with 1% paraformaldehyde in phosphate buffered saline. After dissection, hearts were post-fixated overnight in 1% paraformaldehyde, embedded in paraffin, and 6 µm thick cross-sections at 130 µm spaced intervals were made extending from the apex to the basal part of the left ventricle. Left ventricle (LV) remodeling was assessed by morphometric analysis on mosaic images of Sirius red-stained heart cross-sections using Axiovision 4.6 software (Zeiss, Zaventem, Belgium). LV wall area (mm^2; including the septum), anterior wall thickness, and septal wall thickness were analyzed. All geometric measurements were computed in a blinded fashion from representative tissue sections of 4 separate regions and the average value was used to represent that animal for statistical purposes.
To measure collagen content in the interstitium, Sirius Red staining was performed as previously described by Junqueira *et al.*[13]. Sirius Red polarization microscopy on a Leica RBE microscope with KS300 software (Zeiss) was used to quantify thick tightly packed mature collagen fibers as orange-red birefringent and loosely packed less cross-linked and immature collagen fibers as yellow-green birefringent. Collagen positive area was normalized to the LV remote area and was expressed as percentage. Any perivascular fibrosis was excluded from this analysis. Perivascular fibrosis was quantified as the ratio of the fibrosis area surrounding the vessel to the total vessel area. Two mid-ventricular sections were studied per animal.
Cardiomyocyte hypertrophy was analyzed on paraffin sections stained with rabbit anti-mouse laminin (Sigma; 1/50) by measuring the cardiomyocyte cross-sectional area (μm^2) of at least 200 randomly selected cardiomyocytes in the LV myocardium. Capillary density in the myocardium was determined on CD31 stained sections using rat anti-mouse CD31 antibodies (BD; 1/500). Relative vascularity in the myocardium was

determined as [(capillary density (number/mm^2)/cardiomyocyte density (number/mm^2))/cardiomyocyte cross-sectional area (μm^2)][14]. Two mid-ventricular cross-sections were analyzed per mouse.
Immunostaining for 3-nitrotyrosine was performed with rabbit anti-nitrotyrosine antibodies (Merck Millipore, Overijse, Belgium; dilution 1/250).
Apoptosis was quantified on deparaffinized tissue sections using SignalStain® cleaved caspase-3 IHC detection kit (Cell Signaling Technologies, Beverly, MA), which utilizes a polyclonal rabbit antibody to the neoepitope peptide at the end of cleaved caspase-3[15].

Evaluation of cardiac glucose metabolism by micro-positron emission tomography (micro-PET)-Glucose uptake in the myocardium and in the skeletal muscle was quantified by micro-PET using [^{18}F]-fluorodeoxyglucose (FDG) as a tracer (309 ± 22 µCi). Imaging was performed 60 min after tracer administration. Animals were anesthetized by inhalation of 2% isoflurane in 100% oxygen and underwent static imaging for 10 minutes on a micro-PET Focus 220 scanner (Concorde Microsystems, Knoxville, TN, USA). Images were reconstructed with ordered subset expectation maximization algorithm with 6 iterations (OSEM3D 6i) and analyzed with PMOD v.3.4 (Pmod Technologies, Zurich, Switzerland). To exclude any effect of diurnal variability, micro-PET data acquisition was consistently performed within the same 2 hours' time frame of the day. The simultaneous quantification of skeletal SUVs was performed since myocardial glucose metabolism is not always parallel to skeletal and whole-body glucose metabolism[16].

Micro-magnetic resonance imaging (MRI)-Cardiac micro-MRI was performed under isoflurane anesthesia 8 weeks after sham operation or TAC using a Bruker Biospec, 9.4 Tesla (horizontal bore, 20 cm), small animal MRI scanner (Bruker BioSpin, Ettlingen, Germany) equipped with an actively shielded gradient insert (1200 mT/m) and a 3.5-cm quadrature coil (Bruker Biospin). For localization purposes, 2-dimensional retrospectively triggered (Intragate, Bruker BioSpin) pseudo short-axis and long-axis T1-weighted images were recorded (fast low angle shot, repetition time 6 ms, echo time 1.59 ms, flip angle 15°, matrix 192 x 192, field of view 30 x 30 mm, slice thickness 500 µm; navigator settings: size 76, 1 ms, flip angle 2.5°). A stack of short-axis images (inter-slice distance 1 mm) was then recorded from covering the full heart. Data were reconstructed using Paravision 5.1 (Bruker) by zerofilling to a matrix of 320 x 320 (in-plane resolution 94 x 94 µm) and verifying retrospective triggering accuracy before final reconstruction to 15 frames (using 70% of the respiration signal). Volumes including papillary muscles were derived from manual delineation in ImageJ (http://imageJ.nih.gov/ij; NIH, USA). Myocardial mass was derived assuming a density of 1.053 g/µl.

Statistical analysis-All data are expressed as means ± standard error of the means (SEM). Parameters between four groups were compared by one-way analysis of variance followed by Bonferroni multiple comparisons post-test for comparing sham groups, TAC groups, and sham versus respective TAC groups using GraphPad Instat (GraphPad Software, San Diego, USA). When indicated, a logarithmic transformation or a square root transformation or a non-parametric test was performed. Parameters between two groups were compared using Student's t test. When indicated, a logarithmic transformation, a square root transformation, or a non-parametric Mann-Whitney test was performed. The assumption of Gaussian distribution was tested using the method Kolmogorov and Smirnov. Kaplan-Meier survival curves were analyzed by log-rank test using Prism4 (GraphPad Software). A two-sided p-value of less than 0.05 was considered statistically significant.

SUPPLEMENTAL REFERENCES

1. Jacobs, F, Snoeys, J, Feng, Y, Van Craeyveld, E, Lievens, J, Armentano, D*, et al.* (2008). Direct comparison of hepatocyte-specific expression cassettes following adenoviral and nonviral hydrodynamic gene transfer. *Gene Ther* **15**: 594-603.
2. Lock, M, Alvira, M, Vandenberghe, LH, Samanta, A, Toelen, J, Debyser, Z*, et al.* (2010). Rapid, simple, and versatile manufacturing of recombinant adeno-associated viral vectors at scale. *Human gene therapy* **21**: 1259-1271.
3. Buys, ES, Raher, MJ, Blake, SL, Neilan, TG, Graveline, AR, Passeri, JJ*, et al.* (2007). Cardiomyocyte-restricted restoration of nitric oxide synthase 3 attenuates left ventricular remodeling after chronic pressure overload. *Am J Physiol Heart Circ Physiol* **293**: H620-627.
4. Hu, P, Zhang, D, Swenson, L, Chakrabarti, G, Abel, ED, and Litwin, SE (2003). Minimally invasive aortic banding in mice: effects of altered cardiomyocyte insulin signaling during pressure overload. *Am J Physiol Heart Circ Physiol* **285**: H1261-1269.
5. Weiss, JL, Frederiksen, JW, and Weisfeldt, ML (1976). Hemodynamic determinants of the time-course of fall in canine left ventricular pressure. *J Clin Invest* **58**: 751-760.
6. Jacobs, F, Van Craeyveld, E, Feng, Y, Snoeys, J, and De Geest, B (2008). Adenoviral low density lipoprotein receptor attenuates progression of atherosclerosis and decreases tissue cholesterol levels in a murine model of familial hypercholesterolemia. *Atherosclerosis* **201**: 289-297.
7. Camus, MC, Chapman, MJ, Forgez, P, and Laplaud, PM (1983). Distribution and characterization of the serum lipoproteins and apoproteins in the mouse, Mus musculus. *J Lipid Res* **24**: 1210-1228.
8. Van Veldhoven, PP, Swinnen, JV, Esquenet, M, and Verhoeven, G (1997). Lipase-based quantitation of triacylglycerols in cellular lipid extracts: requirement for presence of detergent and prior separation by thin-layer chromatography. *Lipids* **32**: 1297-1300.
9. Van Veldhoven, PP, Meyhi, E, and Mannaerts, GP (1998). Enzymatic quantitation of cholesterol esters in lipid extracts. *Anal Biochem* **258**: 152-155.
10. Arroyo, AI, Camoletto, PG, Morando, L, Sassoe-Pognetto, M, Giustetto, M, Van Veldhoven, PP*, et al.* (2014). Pharmacological reversion of sphingomyelin-induced dendritic spine anomalies in a Niemann Pick disease type A mouse model. *EMBO Mol Med* **6**: 398-413.
11. Van Veldhoven, PP, and Mannaerts, GP (1987). Inorganic and organic phosphate measurements in the nanomolar range. *Anal Biochem* **161**: 45-48.
12. Lenaerts, I, Driesen, RB, Hermida, N, Holemans, P, Heidbuchel, H, Janssens, S*, et al.* (2013). Role of nitric oxide and oxidative stress in a sheep model of persistent atrial fibrillation. *Europace : European pacing, arrhythmias, and cardiac electrophysiology : journal of the working groups on cardiac pacing, arrhythmias, and cardiac cellular electrophysiology of the European Society of Cardiology* **15**: 754-760.
13. Junqueira, LC, Bignolas, G, and Brentani, RR (1979). Picrosirius staining plus polarization microscopy, a specific method for collagen detection in tissue sections. *Histochem J* **11**: 447-455.
14. Shimizu, I, Minamino, T, Toko, H, Okada, S, Ikeda, H, Yasuda, N*, et al.* Excessive cardiac insulin signaling exacerbates systolic dysfunction induced by pressure overload in rodents. *J Clin Invest* **120**: 1506-1514.
15. Muthuramu, I, Singh, N, Amin, R, Nefyodova, E, Debasse, M, Van Horenbeeck, I*, et al.* (2015). Selective homocysteine-lowering gene transfer attenuates pressure overload-induced cardiomyopathy via reduced oxidative stress. *J Mol Med (Berl)* **93**: 609-618.
16. Nuutila, P, Maki, M, Laine, H, Knuuti, MJ, Ruotsalainen, U, Luotolahti, M*, et al.* (1995). Insulin action on heart and skeletal muscle glucose uptake in essential hypertension. *J Clin Invest* **96**: 1003-1009.